A MODEL OF CAST-IN-PLACE RC PILE INCLUDING REINFORCEMENT SWELLING AND ITS APPLICATION TO EVALUATING THE INFLUENCE OF GROUND MOTION ON PILE FOUNDATIONS

(Translation from Proceedings of JSCE, No. 689/I-57, October 2001)

Masahiro SHIRATO　　Yoshitomi KIMURA　　Jiro FUKUI

When pile foundations experience a severe earthquake, it is generally assumed that postpeak bending behavior emerges locally in the pile at the top and near the boundaries between different soil layers in the ultimate limit state. Experimental results for typical cast-in-place RC piles indicate that the postpeak behavior is mainly caused by the collapse of covering concrete and the local swelling of reinforcing bars. In this paper, we propose a simple constitutive model in which a plastic buckling model is used to describe the swelling of reinforcing bars and which employs a fiber element for the piles. Also we use the plastic buckling length of the reinforcement bar as the element length. Numerical verification using this proposed model shows approximate agreement with experimental results for model piles under cyclic loading. Furthermore, we carry out dynamic analysis using the proposed model of a bridge pile foundation, and propose a design condition and criteria for pile foundations likely to suffer from seismic-induced ground vibration.

Key Words: *pile foundation, postpeak behavior, swelling of reinforcing bar, kinematic interaction, seismic design*

Masahiro Shirato is a research engineer of Foundation Engineering Research Team, Public Works Research Institute, Independent Administrative Institution, Japan. He earned his M. Eng. from Tohoku University in 1997. His main research interests include seismic design of foundations, numerical analysis for soils and foundations and its application to practical design, and limit state design and reliability design of foundations. He is a member of JSCE.

Yoshitomi Kimura is the head of Planning Division, Public Works Research Institute, Independent Administrative Institution, Japan. He earned his M. Eng. from Nagaoka University of Technology in 1987. His research interests include ultimate limit state, ductility design, and reliability design of foundations. He is a member of JSCE.

Jiro Fukui is the team leader of Foundation Engineering Research Team, Public Works Research Institute, Independent Administrative Institution, Japan. He earned his M. Eng. from Osaka University in 1980. He specializes in design, innovative construction technology, maintenance, and reinforcement of foundations, and inspection and countermeasure of effect of scouring on foundations. He is a member of JSCE.

1. INTRODUCTION

In designing infrastructure, accountability for performance during earthquakes is being increasingly required. The concept behind design codes for such structures is changing, with performance-based design becoming more important. Design codes clarify only the performance requirements of structures. In the present Japanese design code for highway bridge foundations, the response to very strong seismic motions of low probability during the service lifetime should be such that no excessive repair work is necessary, thus enabling a quick return to service, and that enough horizontal capacity and ductility are maintained to facilitate repair of damage to the foundations if needed [1], [2]. The Specifications for Highway Bridges [1], [2] in Japan recommends a ductility design method to verify these requirement. This is a static design method, but an inertial force corresponding to the first vibration mode of the seismic response is applied to the superstructure, pier, and footing of the foundation.

In order to investigate quantitatively the stability of pile foundations subjected to such inertial forces from the superstructure and the damage sustained, we have performed a series of large scale experiments and proposed appropriate limiting requirements for the displacement ductility factor of group-pile foundations [2], [3], [4]. This recommended critical ductility factor is considered to be independent of the number of rows of piles and the type of piles as long as the piles satisfy the recommended structural details in the specification, although in practice it is true that the limit ductility factor must depend on those elements. The reason for the recommended limit ductility factor being made constant is that the proposal is based only on a small number of experimental studies, and numerical models and techniques are not sufficiently developed, especially in postpeak behaviors, to allow reliable estimates of the relationship between pile foundation stability and the damage sustained by each pile.

Moreover, recent reports of damage such as that in the Hanshin-Awaji earthquake (Kobe Earthquake) of 1995 suggest that pile foundations are likely to sustain damage near boundaries between soft and hard soil layers because of kinematic interactions between motions of the pile and soil during large earthquakes. Many studies have been carried with the aim of developing prediction methods which are suitable for practical design against such damage [5], [6], [7], [8], [9]. Though it is true that local pile damage and capacity loss resulting from ground vibration during an earthquake are considered to have a minor direct effect on the restoring force of the pile foundations as a system, since pile foundations consist of many piles supported by the ground and are highly statically indeterminate, quantitative prediction methods for the effects of local pile damage and capacity loss and corresponding design methods have not been fully investigated.

In order to develop performance-based design codes/standards, it is necessary to understand the seismic behavior of pile foundations and to clarify the relationship between possible damage state deep in the ground and stability of foundation, just as inertial force has been verified. Unfortunately, experimental investigations face difficulties in simulating dynamic soil-pile interactions under any conditions. On the other hand, numerical approaches are helpful because they can be extended to pile foundations of any design and also any ground conditions. However, we still have been unable to develop an appropriate numerical model for piles that can handle the postpeak behavior of foundations. Cast-in-place RC pile foundations are the most popular type in Japan. Hence it would be quite useful to develop a model which can trace the postpeak behavior of cast-in-place RC piles in order to establish a seismic design concept for such foundations.

Many numerical simulations have been reported to trace the postpeak behavior of RC members [10] and it has been pointed out that the swelling of reinforcement must be properly modeled [11], [12], [13], [14], [15]. Further, some consideration is necessary to avoid mesh size dependency of the numerical results when a softening-type constitutive model is used in finite element analysis [16], [17]. We have carried out experiments on group pile foundations and single piles in air subject to cyclic loading and have reported the progress of damage and postpeak behavior [3], [4]. We also have implemented finite element analysis using a fiber element for the pile to simulate these experiments [18]. As a result, even though the nonlinear characteristics of members are strongly affected by changes in the applied axial load due to the horizontal displacement of the superstructure, we have shown that it is possible to trace the postpeak behavior of foundations numerically as long as each fiber is modeled with the appropriate material nonlinearities and swelling of the reinforcement. As for a general cast-in-place RC pile foundation, however, the problem

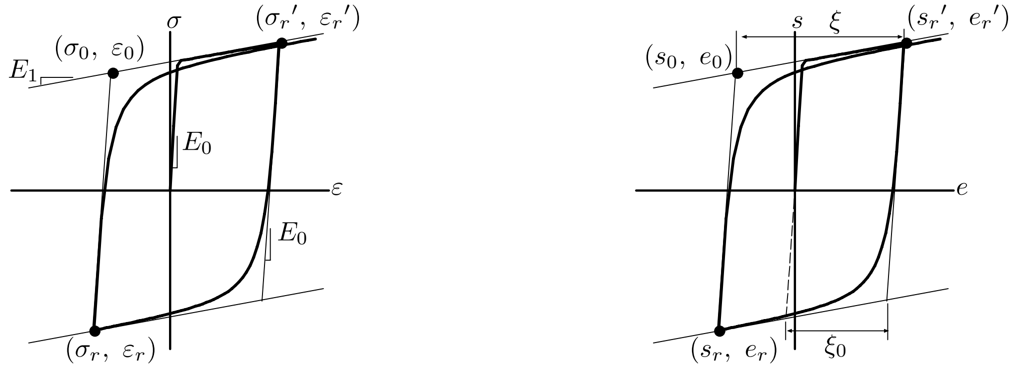

Fig. 1 Menegotto-Pinto model

of how to model the swelling behavior of reinforcement and how to set the element length when using a softening constitutive model in the presence of swelling has not been resolved yet.

In this paper, we first propose a uniaxial constitutive model for longitudinal reinforcement. This can be used with the fiber element representing the pile and can trace the behavior of a cast-in-place RC pile from the elastic region to the postpeak region. We also establish a method of determining the length of elements to which the proposed constitutive model is applied. The proposed model treats the swelling of reinforcement bars as a plastic buckling phenomenon that occurs after compressive collapse of the covering concrete, and this is combined with ordinary constitutive models with no swelling effect. Furthermore, we avoid the element mesh dependency of the results by introduction of the plastic buckling length to the element length. The accuracy and characteristics of this constitutive model are examined through analysis of cast-in-place RC piles subjected to cyclic loading.

Secondly, the seismic behavior of a foundation consisting of cast-in-place RC piles is simulated by dynamic analysis in order to demonstrate the feasibility of the proposed model even in dynamic problems and to clarify the causes of damage to piles deep underground: the relationship between the such pile damage and the stability of pile foundations as a system is also clarified. Finally, we discuss a seismic design method for pile foundations which can take the kinematic effect from seismic-induced ground vibrations into account.

It should be noted that the present analysis dose not take into account the pulling-out of longitudinal reinforcement from the footings. This is because there is inadequate experimental data available to model it, and because the contribution of reinforcement swelling is considered dominant in the post-peak behavior of pile foundations. Only the effect of deterioration in the bending capacity of piles has been examined, while the effect of shear collapse of the piles will be investigated in the future.

2. CONSTITUTIVE MODEL AND ELEMENT LENGTH FOR FIBER MODEL OF PILE

(1) Constitutive model without reinforcement swelling

We employ the Menegotto-Pinto model as a constitutive model for the longitudinal reinforcement, as proposed for the reinforcing bars in RC members subject to cyclic loading.

The Menegotto-Pinto model is specified as a bi-linear behavior with initial rigidity E_0 and hardening rigidity E_1, plus a series of asymptotic curves looking these bi-linear relations as shown in **Fig. 1**. These are given by

$$\sigma^* = b\varepsilon^* + \frac{(1-b)\varepsilon^*}{(1+\varepsilon^{*R})^{1/R}} \tag{1}$$

with definitions

$$\sigma^* \equiv \frac{\sigma - \sigma_r}{\sigma_0 - \sigma_r}, \quad \varepsilon^* \equiv \frac{\varepsilon - \varepsilon_r}{\varepsilon_0 - \varepsilon_r}, \tag{2}$$

where σ is stress; ε is strain; $(\sigma_r, \varepsilon_r)$ is the last strain reversal point, and $(\sigma_0, \varepsilon_0)$ is the intersection of the two envelopes when unloading and loading occurs from point $(\sigma_r, \varepsilon_r)$ as illustrated in **Fig. 1**. Parameter b is a hardening ratio defined by the initial rigidity E_0 and the hardening rigidity E_1 as follows.

$$b \equiv E_1/E_0. \tag{3}$$

Parameter R represents the deviation of a stress-strain branch from the bi-linear curve and is defined by

$$R = R_0 - \frac{a_1 \xi}{a_2 + \xi} \tag{4}$$

where R_0, a_1, and a_2 can be regarded as material constants, and R_0 is the value of R at initial yield. We here give the same values to R_0, a_1, and a_2 as used in numerical analysis of cast-in-place RC piles by Shirato et al. [18], because no experimental data is available to determine these material parameters. Parameter ξ is defined by

$$\xi \equiv |\varepsilon_0 - \varepsilon_r{}'|/\varepsilon_y = |e_0 - e_r{}'|, \tag{5}$$

where $\varepsilon_r{}'$ represents the preceding maximum or minimum strain reversal point with respect to $(\sigma_r, \varepsilon_r)$. This parameter represents the absolute value of plastic strain developed from $(\sigma_r, \varepsilon_r)$ to $(\sigma_r{}', \varepsilon_r{}')$, and is updated at every unloading and loading step, where $\sigma_r{}'$ is the corresponding stress to $\varepsilon_r{}'$. Here we use the definition in **Fig. 1** as

$$s \equiv \sigma/\sigma_y, \quad e \equiv \varepsilon/\varepsilon_y, \tag{6}$$

where σ_y and ε_y stand for the initial yield stress and strain respectively. In the application of Eqs. (4) and (5), if partial unloading and reloading occurs, we calculate the value of ξ by using the strain reversal points during the unloading and reloading branch. Note that ξ at first strain reversal is estimated as illustrated in **Fig. 1**.

(2) Criteria for initial swelling

It is easy to understand that there exist some interactions between reinforcement swelling and collapse of the covering concrete. For example, Suda et al. [11], [12] have generalized the mechanism of the initiation of reinforcement swelling and proposed a criterion for the appearance of swelling with consideration of such an interaction.

However the results of existing loading tests on model cast-in-place RC piles [3], [4], [21] suggest that the covering concrete is crushed or falls apart when the capacity of the piles begins to drop significantly owing to bending. Therefore we consider it appropriate to employ a simple assumption that reinforcement swelling does not occur until the covering concrete at the position of the reinforcement bar collapses. In detail, swelling becomes possible if the following conditions are satisfied consecutively:

1. first the strain of the reinforcement bar exceeds the compressive failure strain of the covering concrete,
2. then the reinforcement bar undergoes unloading or tensile loading, and
3. finally the reinforcement bar undergoes compressive loading again.

That is, the swelling of reinforcements is never initiated under monotonic loading.

(3) Constitutive model and length of fiber elements for reinforcement bar with swelling

Fig. 2 illustrates the proposed constitutive model taking swelling into account. This model consists of two parts, one of which is the Menegotto-Pinto model without swelling (curve ABC), and the other being a load-displacement curve indicated by PQBR where a longitudinal reinforcement bar buckles plastically at point 'Q'. The abscissa of this figure is the averaged strain over the characteristic buckling length which depends on the arrangement of reinforcement in each pile.

Curve PQBR is assumed to be derived by plastic buckling analysis in two dimensions of a longitudinal reinforcing bar supported by hoop bars and core concrete, as is shown in **Fig. 3**. F and u in **Fig. 3** denote the vertical load and displacement at the loading point, respectively. The hoop resistance is modeled by a

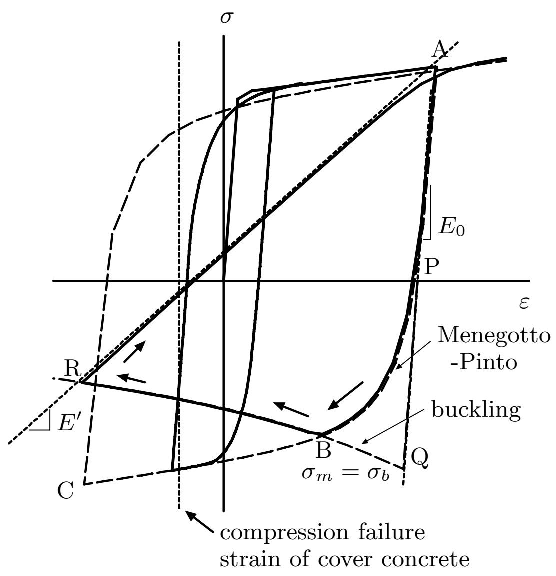

Fig. 2 Constitutive model including the swelling effect of reinforcement bars

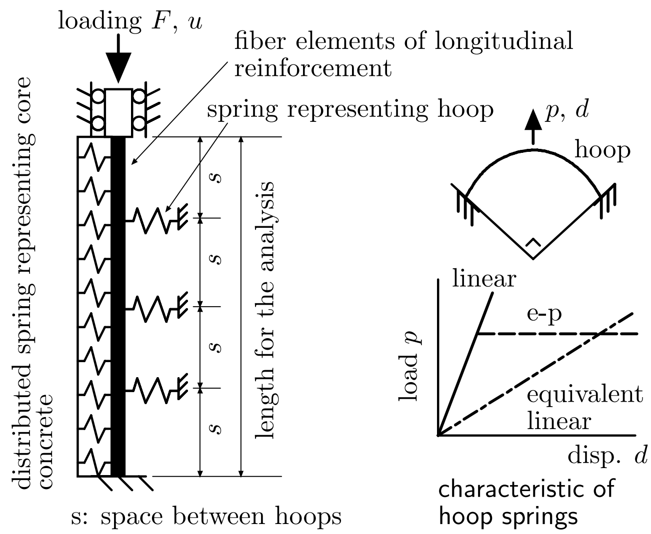

Fig. 3 Numerical analysis of plastic buckling of reinforcement bar (in case $L = 4s$)

series of discrete springs with a spacing equal to that of two adjacent hoop reinforcements, while the core concrete is replaced by uniformly distributed elastic springs. Note that the resistance of the latter springs is non-zero only when the displacement of the longitudinal reinforcement is toward the core concrete side. Horizontal and vertical displacement and rotation at the bottom are fixed, and horizontal displacement and rotation at the top are also fixed. Details of using this model will be given in Section **3.** together with the results of plastic buckling analysis.

It is easily imagined that plastic buckling behavior will depend on the model length of the reinforcement analyzed. But, Suda et al. [11], [12], for example, have suggested a method of estimating the plastic buckling length properly; here the elastic buckling of a bar on an elastic foundation is employed but the corresponding flexural rigidity is modified step by step depending on the degree of development of the plastic region under a certain loading.

However, we here propose a new method that is suitable for the practical implementation. First, we numerically perform several cases of plastic buckling analysis on reinforcement of length $L = ms$, where m is an integer to be controlled and s is the spacing between two adjacent hoops. Then we determine the critical m_0; that is, the characteristic plastic buckling length $L_0 = m_0 s$ at which the most drastic fall in load is observed after initiation of plastic buckling among many trials with different m's. It should be noted that there exist $(m-1)$ sets of springs for a bar of length $L = ms$. Dividing the obtained load F by the cross sectional area of the reinforcement and also dividing the displacement u by the characteristic plastic buckling length $L_0 = m_0 s$, we obtain the normalized and averaged stress-strain relation. Finally this averaged stress-strain relationship is adopted to express the compressive branch of the stress-strain relation curve PQBR in **Fig. 2** by referring to the method employed by Gomes and Appleton [15]. Point 'P' is where the elastic unloading path of rigidity E_0 from the maximum tensile strain point 'A' in the history crosses the zero stress level. Note that, in the analysis of pile behavior later on, we assume a piecewise linear load-displacement relationship for buckled longitudinal reinforcement and interpolate the discretized load-displacement data obtained from numerical analysis of plastic buckling of the reinforcement.

Swelling is assumed to occur when compressive stress σ_m derived from the Menegotto-Pinto model and σ_b obtained from the curve PQBR become coincident at a certain strain level. Thus, the stress-strain response chooses curve B-R not along path B-C of the Menegotto-Pinto model.

When strain reverses after the post buckling branch and becomes an expansion, the stress and strain response begins to tend toward the maximum tensile strain point of the history, as proposed by Shirato et al. [18] This implies that the tensile resistance of longitudinal reinforcement bars that have experienced swelling under compression becomes smaller than in the virgin state without any swelling. In the numerical analysis of pile behavior below, we set the value of E_0 to E', which is the instantaneous modulus between 'R' and 'A' (i.e. between the strain reversal point in the compression branch and the maximum tensile strain point in the history), and set the curvature parameter $R = R_0$ in the Menegotto-Pinto model.

The length of the fiber elements into which the proposed constitutive model is installed must be made equal to the characteristic plastic buckling length L_0, as used in the setting of the curve PQBR. This is because we want to reflect the physical phenomena onto the element length through averaging the deformation within the element.

Judging from the results of past experimental research [3], [4], [21], we can expect the length of the swelling portion of the reinforcement in the standard arrangement to be approximately a half of the diameter of the pile. From this, it can be easily imagined that axial extension and compression will not occur simultaneously in one particular fiber of the element as long as the element length is of the same order, so our proposed method is considered applicable here. Since, in general, real piles are in practice around ten diameters in length or more, sufficient accuracy is possible from the viewpoint of convergence in the FEM analysis. Note that it is possible to apply the proposed model for handling the swelling effect to any constitutive model as long as it is described within the framework of deformation theory.

(4) Constitutive model of concrete

Since the focus here is the postpeak behavior of pile foundations subjected to cyclic loading, we employ the so-called modified Muguruma model proposed by Ristic et al. [20], which can handle softening behavior due to cyclic motion.

However, we modify this model further as follows, and construct a skeleton curve as is illustrated in **Fig. 4**. The maximum compressive stress point (CC) is evaluated and then the degradation gradient (CC-U) using the model by Hoshikuma et al. This takes the confining effect of the hoop reinforcement into account for standard columns and piles, and is adopted in the Specifications for Highway Bridges [1]. This modification alters the skeleton curve of the modified Muguruma model so that it no longer possesses a sustaining branch of peak strength . Further, since the descending gradient introduced by Hoshikuma et al. is evaluated through regression analysis of results obtained uniaxial compression tests with large-scale specimens in the range from maximum compressive strength σ_{cc} to $0.5\sigma_{cc}$, it cannot be applied directly to this model. Accordingly we derive the first descending gradient which is valid in the range from σ_{cc} to $0.5\sigma_{cc}$ (the branch CC-U) from Hoshikuma et al., and we further assume that the second descending gradient in the range below $0.5\sigma_{cc}$ (the branch U-L) is half of the first one.

Since the constitutive laws of concrete also include softening, similar treatment to that used for the constitutive relation of reinforcement needs to be applied to the constitutive relation of concrete in order

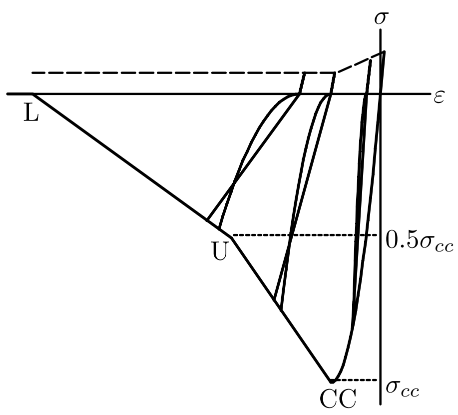

Fig. 4 Schematic outline of constitutive model of concrete employed in this paper

to avoid mesh size dependency in the numerical results. Although many reports exist on this subject, there is no well-established method of solving this problem. Therefore we here employ the model proposed Hoshikuma et al. without any modification [16].

3. PLASTIC BUCKLING ANALYSIS OF REINFORCING BAR

(1) Numerical model for plastic buckling analysis

Now we carry out a series of plastic buckling analyses of reinforcing bars constrained by core concrete and hoops, as is illustrated in **Fig. 3**. The 2D finite element method is employed within a framework of finite displacements. A reinforcing bar is expressed by a group of fiber elements; that is, the cross section is divided into a number of layer-like elements.

We adopt the Menegotto-Pinto model as the constitutive model for each fiber of a reinforcing bar. Although it would be possible to use other models, rather than the Menegotto-Pinto model originally developed for the analysis of RC members subject to cyclic load, for consistency of analysis we employ the same model as used for the analysis of the behavior of cast-in-place RC piles, as mentioned later. The spring constant of the spring representing the hoop resistance is obtained through a series of separate finite element analyses of an arch model subjected to a normal force at the top, as shown in **Fig. 3**. In this model, the arch consists of a hoop reinforcement with both ends fixed and an open angle of 90 degrees. The distributed spring used to model the resistance of the core concrete does not resist tensile force, and the compressive spring constant is set just large enough to prevent the longitudinal reinforcement from penetrating into the core concrete.

The reinforcing bar is divided into ten elements in the longitudinal direction, and the cross section is modeled by 50 fiber elements. A distributed concrete spring is located at each node. Finally a small initial parabolic imperfection is introduced into the longitudinal reinforcing bar so that buckling can be triggered easily.

(2) Determination of plastic buckling length of reinforcing bar

Two model cast-in-place RC piles are examined in this paper. These have been the subject of model tests in experiments where the behavior of piles subject to horizontal cyclic loading was examined. The numerical analysis is presented in Section **4.** The dimensions of the model piles are summarized in **Figs. 10** and **15**. We refer to the first as the type-1 pile specimen and to the latter pile as the type 2 pile specimen. Material constants and parameters for the Menegotto-Pinto model are chosen to be identical with those employed in the analysis of the experiments described in Section **4.**

First, assuming that the hoops never yield, we obtain spring constants k_r which represent the hoop resistance by finite element analysis of the arch model shown in **Fig. 3**. The value of k_r for the type-1

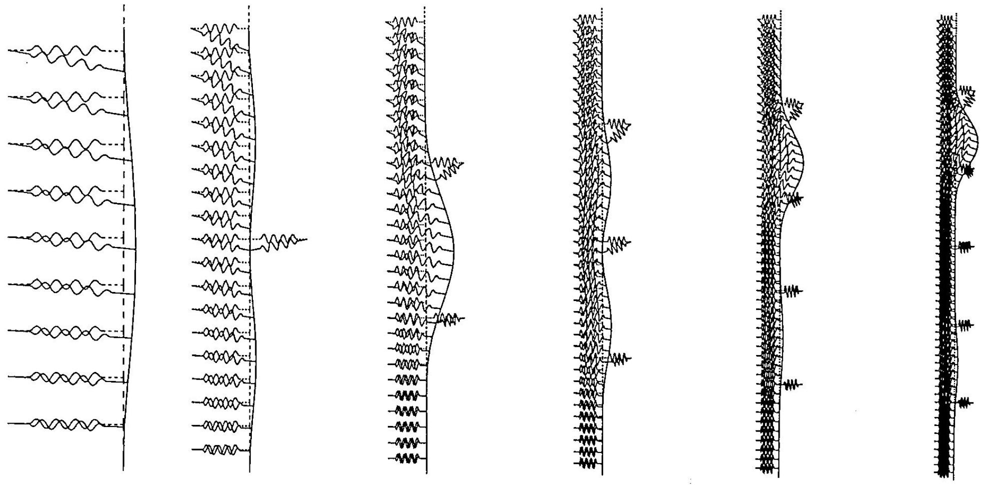

$L/s = 1$ $L/s = 2$ $L/s = 3$ $L/s = 4$ $L/s = 5$ $L/s = 6$

Fig. 5 Deformed shape after plastic buckling of longitudinal bar in type-1 pile specimen

pile specimen is 1.7 MN/m, and it is 19.0 MN/m for the type-2 specimen. The spring constant of the distributed spring representing the core concrete must be sufficiently rigid; it is set at 9.8 GN/m^2. As explained in Section **2.(3)**, plastic buckling analysis of reinforcing bars of length $L = ms$ with various values of m is executed in order to determine the critical value $m = m_0$ which leads to the most unstable load-displacement history.

As for the type-1 pile, six cases denoted $m = 1, 2, \cdots 6$ are analyzed. **Fig. 5** illustrates the initial states by dashed lines and the corresponding deformed configurations at an average strain of 5% by solid lines. The average strain is defined by the longitudinal displacement at the loading point per length L. The scale of each figure is also normalized by the length L. The springs are shown schematically in there figures, with both the initial and deformed states shown. The springs do not resist displacement of reinforcing bars in the longitudinal direction. The deformed configurations suggest that the buckling mode when $L = 5s$ and $6s$ is the same as when $L = 3s$.

Fig. 6 shows the relationship between vertical load and displacement normalized by buckling mode in order to estimate the load-displacement relationship for each buckling mode. In all cases, buckling occurs immediately after initial yielding of the material.

Then, as can be expected from the buckled shape, the results for cases $L = 3s$, $5s$, and $6s$ are similar to each other, and they show a most significant drop in load-carrying capacity. The length of the swelled portion of the longitudinal reinforcement bars observed in the experiments shown in **Photo 1** is approximately $3s$, and this agrees well with the most unstable response obtained in this series of buckling analyses.

As for the type-2 pile, similar results are obtained as summarized in **Fig. 7**. The deformation configuration when $L = 3s$ is also drawn in this figure.

In comparison with the experimental results in **Photo 2**, the shape of the swelling when $L = 3s$ coincides with the experimental observations well. In this type-2 pile, the buckling mode at $L = 5s$ is also the same as that at $L = 3s$. Although there are differences in reinforcement arrangement between the type-1 and type-2 pile specimens, the buckled shape corresponding to the most drastic drop in the load-displacement curve is more or less the same as that observed experimentally.

These results indicate that plastic buckling is initiated by loss of bending stiffness due to plasticization of the cross section, and that the buckling load is independent of length L. On the other hand, buckling mode and post-buckling behavior depend on length L. However a comparison with experimental results

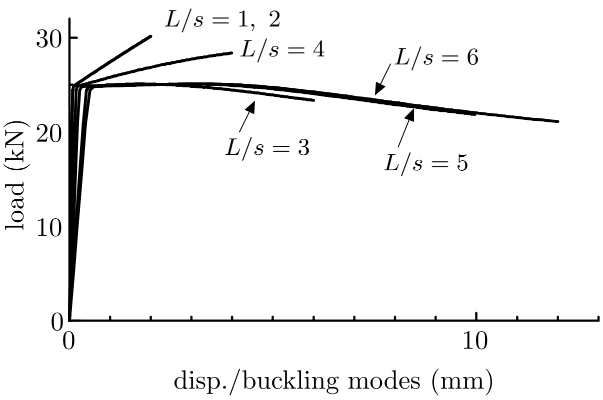

Fig. 6 Normalized load-displacement relationship (type-1 pile specimen)

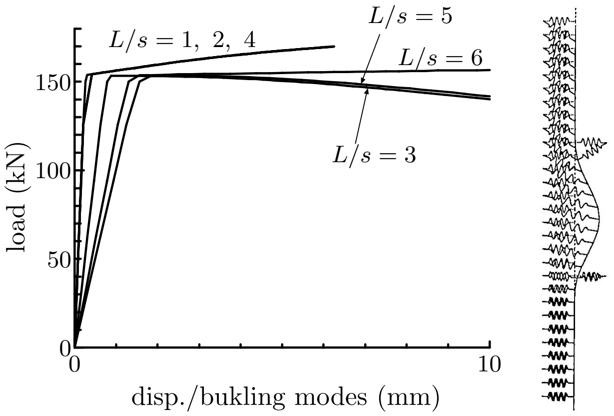

Fig. 7 Normalized load-displacement relationship and plastic buckling deformation for case $L = 3s$ (type-2 pile specimen)

for real piles suggests that the actual swelling phenomena are strongly governed by the buckling mode where the most drastic drop in the load-displacement curve occurs.

(3) Differences in reinforcing bar behavior due to variations in hoop resistance spring rigidity

Although it is assumed in the plastic buckling analysis above that the hoop reinforcement remains elastic, it can also be imagined that it may yield if the horizontal swelling deformation of the reinforcement bars becomes excessive. In order to examine such a possibility and its sensitivity to the plastic buckling behavior of the longitudinal reinforcements, we here try to analyze the response for three different definitions of the springs representing the hoop resistance, with the length to be analyzed fixed at $L = 3s$:

- it is an elastic spring (as in Section **(2)**),
- it is an elastic and perfectly-rigid plastic (e-p) spring whose yield point is defined by the state when the outermost fiber of the arch model of the hoop yields first, and
- it is an equivalent linear spring with spring constant k_{fe}, which is the secant elastoplastic modulus of a spring at the point where the longitudinal reinforcement undergoes vertical compressive deformation at $0.1L$ in the plastic buckling analysis with the elastic-perfect plastic springs. In this case, eventually, $k_{fe} = k_f/3$ in the case of the type-1 pile specimen, while $k_{fe} = k_f/1.4$ in the type-2 pile,

where it is supposed that the spring constants of the equivalent linear spring become so small that the results of the assessment of the performance of piles can lay on safety side. In this analysis for length $L = 3s$, only two springs for the hoops are included and arranged symmetrically with respect to the central node in the longitudinal direction of the reinforcing bar. Therefore both the springs deform quite similarly throughout the numerical analysis of plastic buckling.

Fig. 8 shows the results for the reinforcement in the type-1 pile specimen. In this case, the three models of the hoops yield completely different post-buckling behavior. The influence of the load-displacement curve model of the buckled longitudinal reinforcement on the behavior of the pile will be examined in the next section. On the other hand, the type-2 case shown in **Fig. 9** exhibits no apparent difference due to choice of hoop model. Note that we have also elucidated other characteristics of post-buckling behavior that depend on the hardening ratio, etc. A corresponding detailed discussion of such examinations can be found in a separate reference by Shirato et al. [23]

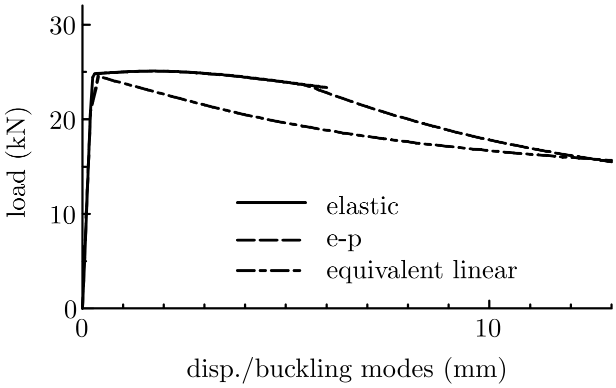

Fig. 8 Difference in normalized load-displacement relationship caused by different spring constants for hoop resistance (type-1 pile specimen, $L = 3s$)

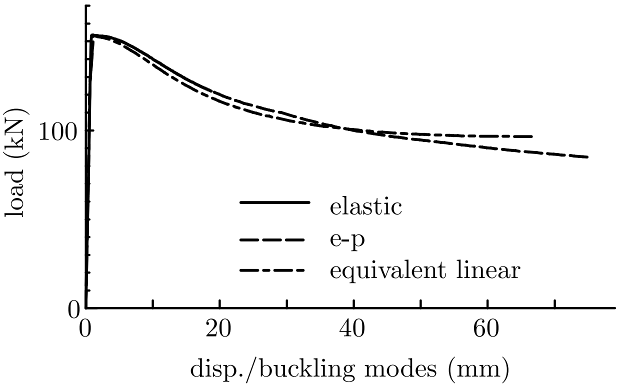

Fig. 9 Difference in normalized load-displacement relationship caused by different spring constants for hoop resistance (type-2 pile specimen, $L = 3s$)

4. NUMERICAL ANALYSIS OF CAST-IN-PLACE RC PILE SPECIMENS SUBJECTED TO REVERSED CYCLIC LOADING

In order to verify the validity of the proposed model, experimental results obtained for cast-in-place RC piles subjected to cyclic loading will be numerically simulated using the model. Experiments in which swelling of the reinforcing bars occurred due to bending are examined here. The scale of the model specimens tested is large enough for them to be actual piles, and the specimens contain almost the same ratio of longitudinal reinforcement as actual piles.

We use a two-dimensional finite element method within the framework of infinitesimal displacement theory. Each longitudinal reinforcing bar in the pile is modeled by a single fiber element. Aside from the reinforcement, the cross section of the pile itself is first divided into 50 layers and then each layer is subdivided again into fibers of core concrete and covering concrete.

(1) Experiment on type-1 pile specimen subject to horizontal reversed cyclic loading with a constant axial load

a) Summary of experiment

We here refer to the experiment on type-1 pile specimens performed by Kimura et al. [3], [4]. The specimens are summarized in **Fig. 10**. The corresponding material properties obtained from standard element tests are listed in **Table 1**. The axial load was first applied to the top of the specimen up to 147 kN and maintained there throughout the experiments. The horizontal reversed cyclic load was then applied. This cyclic loading was controlled by displacement at the horizontal loading point of the specimen. The amplitude of the specified displacement was gradually increased from δ_y to $n \times \delta_y$ ($n = 2, 3, 4, \cdots 16$), where the yield displacement δ_y is defined as the displacement at which an extreme longitudinal reinforcement bar first yields. It was eventually determined to be 3.57 mm in this specimen of their experiments. At each displacement, three cycles were repeated.

Fig. 11 shows one horizontal load-displacement history measured at the loading point in the experiment. Noteworthy characteristics of this history are summarized as follows. Horizontal cracks appeared when the horizontal load reached 24.5 kN, and the maximum horizontal load, 55 kN, was attained when the horizontal displacement became $4\delta_y$ (14.3 mm). During the $5\delta_y$ cycle, the surface concrete of the pile collapsed near the joint between the pile and the footing. Although the horizontal load fell temporarily during the $7\delta_y$ cycle (25.0 mm), it was maintained afterwards in cycles $7\delta_y$ through $10\delta_y$. However loss of horizontal load started again at cycle $10\delta_y$ (35.7 mm), and damage to the pile became noticeable. Eventually, at cycle $13\delta_y$, several large pieces of the covering concrete suddenly dropped away. Thereafter,

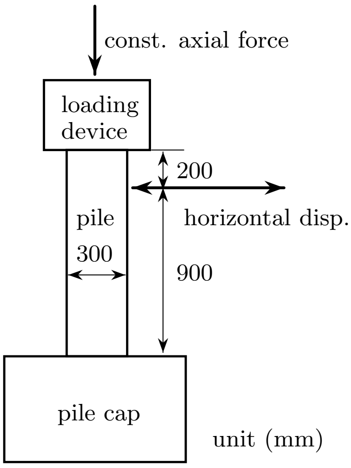

longitudinal reinforcement	SD295A 16-D10
hoop reinforcement	SD295A D4 ctc 40
σ_{ck}	27.1 N/mm^2
distance from surface of pile to center of longitudinal reinforcing bar	50 mm

Fig. 10 Experiment on type-1 pile specimen subject to horizontal reversed cyclic loading

Table 1 Results of material element tests for type-1 pile specimen

reinforcement

reinforcement	yield stress (N/mm^2)	tensile strength (N/mm^2)	Young's modulus (kN/mm^2)
longitudinal	348	478	175
hoop	389	554	213

concrete

age (days)	compressive strength (N/mm^2)	Young's modulus (kN/mm^2)	splitting strength (N/mm^2)
40	27.1	26.5	2.72

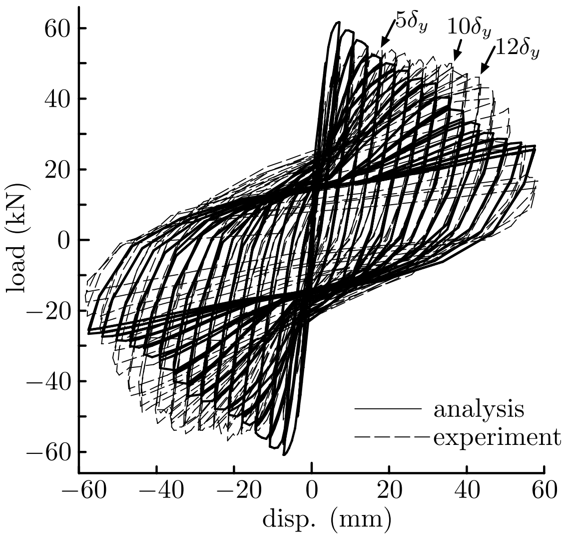

Fig. 11 Horizontal load-displacement hysteresis at the loading point (type-1 pile specimen)

the reinforcement began to fracture at $14\delta_y$, and the experiment was terminated after the $16\delta_y$ cycle (57.1 mm). Observed damage near the bottom of the specimen is shown in **Photo 1**. The longitudinal reinforcement bars swelled in the shape of a sinusoidal wave with a wavelength approximately three times as long as the distance between two adjacent hoops (120 mm).

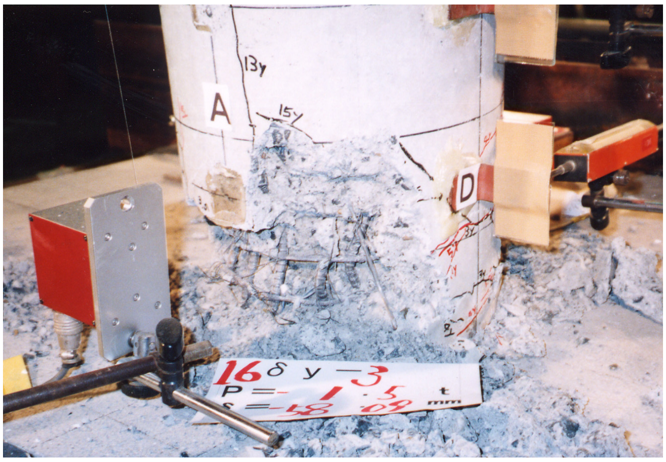

Photo 1 Damage at bottom of type-1 pile specimen after the experiment

b) Numerical analysis model

We model the specimen as a cantilever beam whose fixed end represents the footing. An element length of $3s$ (120 mm) is chosen because this is the smallest size which results in an unstable load-displacement relation among those tested in the plastic buckling analysis in Section **3.(2)**.

In order to check the effects of various types of post-buckling behavior of the reinforcement arising from differences in the spring representing the hoop resistance on predicted pile behavior, two kinds of averaged stress-strain relation of the plastic buckled reinforcement in **Fig. 8** are tested; one is obtained by using the equivalent linear spring, and the other using the elastic and perfectly-rigid-plastic spring. The cross-sectional area of the longitudinal reinforcement bars is as given in the JIS code, while the necessary material parameters are determined by element tests. However, since the hardening ratio b of the Menegotto-Pinto model is not available, it is assumed to be one hundredth of the initial (elastic) rigidity, which is obtained from a standard tensile test of the longitudinal reinforcement in a type-2 pile specimen (SD345).

Also, since it is difficult to choose appropriate material parameters for the covering concrete, we carry out a parametric study for the type-1 pile without consideration of the swelling effect [18]. The parameters which yield relatively good accordance with the experimental results are used; i.e. the envelope of load-displacement hysteresis up to the $10\delta_y$ cyclic loading. In this parametric study, the confinement of covering concrete by the hoops is not taken into account, and the first descending gradient from σ_{cc} to $0.5\sigma_{cc}$ is 1.5 times as steep as that of the core concrete. Note that we may have some problems due to the chosen constitutive concrete relation, as discussed in Section **2.(4)**, because the difference between element lengths used in the numerical simulation here and in the numerical examination in the reference [18] is approximately 20 %.

Loading in the numerical simulation also begins with application of a vertical load of 147 kN at the top of the pile. Then the horizontal cyclic displacement history is applied.

c) Numerical results and discussion

In order to examine the accuracy of our numerical analysis in predicting softening behavior, we first discuss the results of a case employing the stress-strain relation of a buckled longitudinal reinforcing bar, obtained by using equivalent linear springs for the hoops. This case sustained a sudden drop in resistance of the longitudinal reinforcement after yield, as shown in **Fig. 8**. This case is selected to check the feasibility of our numerical model, because the strength of the reinforcing bar falls immediately after buckling begins and the estimated strength is lower than that obtained under the assumption of elastic perfectly-plastic springs. The calculated horizontal load-horizontal displacement history at the loading point is shown in **Fig. 11** together with the experimental results.

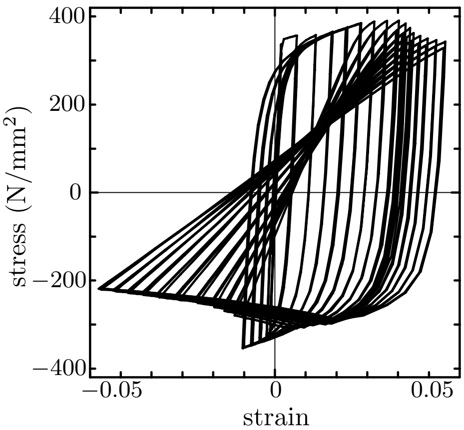

Fig. 12 Stress-strain hysteresis of typical outermost longitudinal reinforcement bar placed at the bottom of a pile

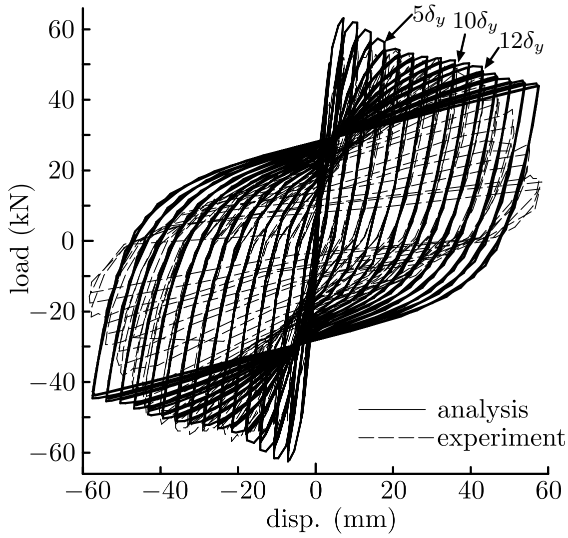

Fig. 13 Horizontal load-displacement hysteresis at the loading point for case without considering swelling of reinforcing bars (type-1 pile specimen)

The numerical analysis overestimates the loads up to the $4\delta_y$ cycle as compared with the experimental data. After that, swelling of the outer reinforcement begins in the $6\delta_y$ cycle, resulting in rapid reduction in the load. In the experimental results, this was observed during the 10 to $13\delta_y$ cycles. However the outlines of the inner loops of the load-displacement relationships closely fit the experimental ones at each cycle $n\delta_y$.

Fig. 12 shows the hysteresis loops of the longitudinal stress-strain relation at the center of a typical outmost reinforcement bar in the element at the bottom. Swelling begins at the $6\delta_y$ cycle. The peak tensile stress at each step decreases as the pile deformation becomes greater. This indicates a progressive accumulation of residual swelling deformation, and it is in good agreement with experimental observations, as seen in **Photo 1**.

For the sake of comparison, another numerical result of the Menegotto-Pinto model reinforcement without swelling is illustrated in **Fig. 13**. This model is referred to as the conventional model. Note that the element length employed in this reference calculation by Shirato et al. [18] is different from the present one, and is one half of the diameter of the pile specimen (150 mm). Since, except for this difference in element length, both analyses handle the same pile systems, the envelope curves obtained in **Figs. 11** and **13** are very similar. Further both calculated envelopes are larger than the experimental data from cycle 1 through to $4\delta_y$. After the $4\delta_y$ cycle, as far as the shape of the envelopes is concerned, the simulations agree relatively well with the experiments up to the $10\delta_y$ cycle. This is of course because the material parameters of the covering concrete are determined by trial and error [18] so that the numerically obtained envelope curves offer a good coincidence with those in the experiments, at least below the $10\delta_y$ cyclic level.

However, the conventional model is unable to predict phenomena such as the excessive decrease in load observed in cycles over $10\delta_y$ in the experiments, and ultimately it overestimates the ultimate strength. Moreover, the conventional model does not reflect the pinching phenomenon often observed in the experiments, while our proposed model can. Judging from these comparisons, we must conclude that reinforcement swelling plays a very important role in the deformation history of piles at large displacements, and particularly the transition to rapid loss of load-carrying capacity and the shape of the inner loops of the hysteresis response.

Even the proposed model, however, has several problems. For example, the load is overestimated up to the $4\delta_y$ cycle, and the capacity of the pile rapidly decreases at a much earlier loading stage (at the $6\delta_y$ cycle) than indicated in the experimental results. These numerical characteristics result from the constitutive

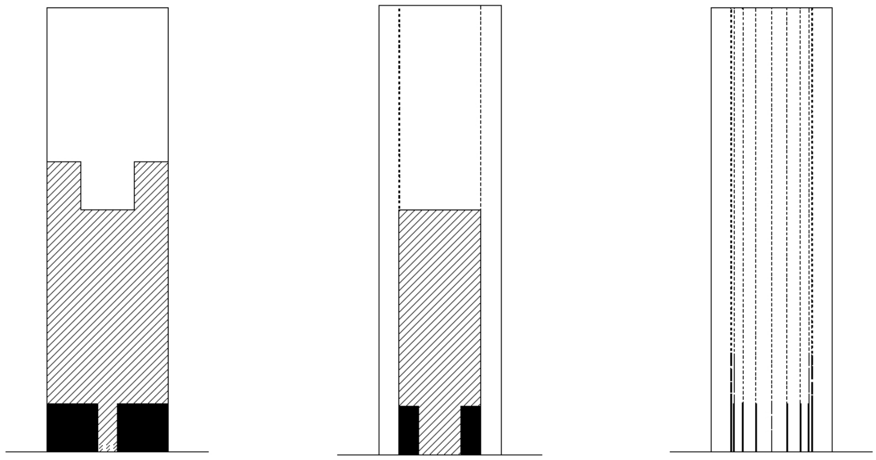

Fig. 14 Damage state immediately after the final $13\delta_y$ cycle

law used for the covering concrete, especially its skeleton curve. Of course, Young's modulus and the maximum compression strength of the constitutive model strongly influence the predicted load at early stages of the loading history and the maximum strength of the pile. Moreover, the descending gradients of the resistance curves also have an extraordinary effect on the loss of load-carrying capacity, since collapse of the covering concrete is one necessary condition for the development of reinforcement swelling.

In the numerical analysis, while the covering concrete fractures at a typical outermost longitudinal reinforcing bar at the $5\delta_y$ cycle near the base of the pile, the core concrete experiences compressive failure during the $10\delta_y$ cycle. On the contrary, in the experiments, only slight damage is observed on the surface at the $5\delta_y$ cycle, and excessive damage to the covering concrete starts after approximately the $12\delta_y$ cycle. Namely, in the numerical analysis, the initiation of swelling of the outmost reinforcement occurs at the $6\delta_y$ cycle as shown in **Fig. 12**, at which point the covering concrete provides adequate confinement in the experiments.

Fig. 14 is a side view of the specimen in a schematic form, showing damage to the fibers obtained numerically after the final $13\delta_y$ cycle. In the two left-hand diagrams, the areas with hatching indicate portions that experience tension cracks, while black areas represent concrete where compressive collapse occurs. In the diagram on the right, the dotted lines represent the positions of longitudinal reinforcement, the areas filled with dashed lines are the yielded zones, and those filled with solid lines are the swelled sections. Compressive failure of the concrete and reinforcing bar swelling occurs only in the bottom elements; the element length is set at three times the spacing between two adjacent hoops (120 mm). These characteristics in the longitudinal direction coincide well with those observed in the experiment, as seen in **Photo 1**. On the other hand, in the cross-sectional direction, concrete damage progress is quite different in the numerical simulation and the experiment. **Photo 1** of the experiment shows that the damage does not penetrate across the position of the outmost reinforcement bars into the core section, while the damage numerically obtained and shown in **Fig. 14** expands into the inner region of the core concrete, and accordingly all the reinforcing bars except the central ones buckle. The conclusion must be that numerical analysis predicts excessive extension of the damage.

At the end of the numerical analysis of the type-1 pile specimen, we carry out the numerical simulations using the elastic and perfectly-plastic springs for the hoop resistance in order to evaluate the different stress-strain curve of the buckled longitudinal reinforcement. However, there is no noticeable difference with the results in **Fig. 11**, and the size of the discrepancy is no more than a few percent. This suggests that differences in the nonlinear properties of hoop resistance do not cause serious variations, probably because the influence of the covering concrete model chosen on the overall properties of the piles is significantly larger than that of other factors.

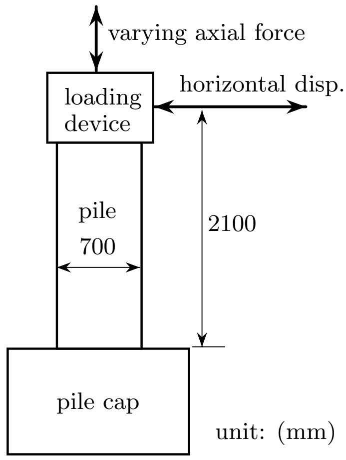

longitudinal reinforcement	SD345 20-D22
hoop reinforcement	SD345 D4 ctc 125
σ_{ck}	23.7 N/mm^2
distance from surface of pile to center of longitudinal reinforcing bar	100 mm

Fig. 15 Experiment of type-2 pile specimen [24]

Table 2 Results of material element tests of type-2 pile specimen

reinforcement

reinforcement	yield stress (N/mm^2)	tensile strength (N/mm^2)	Young's modulus (kN/mm^2)	extension (%)
longitudinal	397	589	195	23.2
hoop	397	569	189	22.8

concrete

age (days)	compressive strength (N/mm^2)	Young's modulus (kN/mm^2)	splitting strength (N/mm^2)
10	23.7	21.9	2.4

(2) Experiment on type-2 pile specimen subject to horizontal reversed cyclic loading and varying axial load

a) Summary of experiment

The type-2 pile specimen chosen for our examinations is the cyclic loading test of a model cast-in-place RC pile performed by Tanamura et al. [24] A summary of this experiment and the results of standard element tests are shown in **Fig. 15** and **Table 2**, respectively. A specimen of this size can be considered a very large model, since more than 80% of cast-in-place RC piles used for highway bridges in Japan are either ϕ1000 or ϕ1200 in diameter [25]. Horizontal loading was controlled by displacement, with the drift angle defined by the ratio of horizontal displacement applied at the loading point to the shear span specified as follows: after consecutive cycles at an angle of 1/1000 and 1/400, once at each magnitude, the amplitude was gradually increased ten times from 1/200 to 10/200 in steps of 1/200 and three cycles were applied at each magnitude.

One of the most noteworthy features of this experiment is that the pile was also subjected to an axial force which varied accordingly to the horizontal reaction force, as depicted by the dashed lines in **Fig. 16**. This loading condition was employed in order to simulate the actual loading states observed in group-pile foundations subjected to horizontal displacement during earthquakes.

Photo 2 shows the damage states visible after the test. The longitudinal reinforcement bars swelled greatly between two adjacent hoops, and so did the hoops to some extent. **Fig. 17** illustrates the horizontal load-horizontal displacement hysteresis at the loading point. The experimental results can be summarized as follows. The covering concrete collapsed on the compressive side of the pile at the bottom when the axial force increased in the compressive direction during the cycle with a drift angle of 2/200. When the

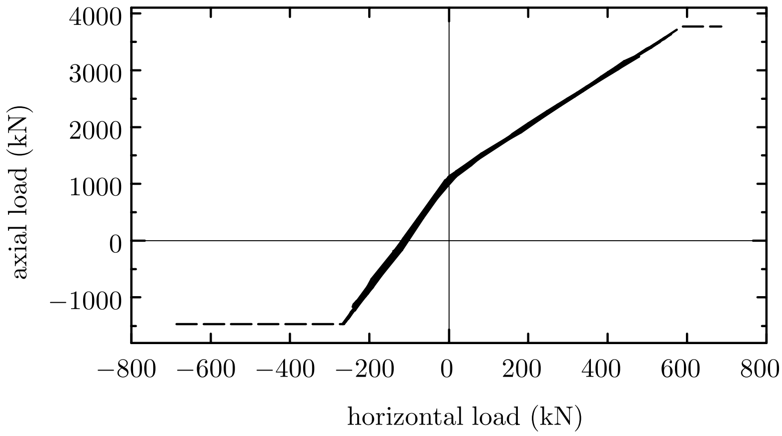

Fig. 16 Varying pattern of axial load (dashed lines) [24]; compression is positive. Solid lines indicate the numerical results.

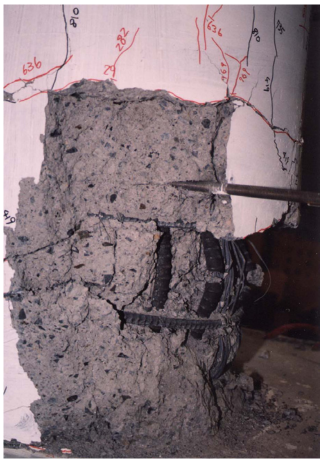

Photo 2 Damage at bottom of type-2 pile specimen after the experiment (compressive side when the pile was subject to compressive axial force)

displacement was reversed in the same cycle, the longitudinal reinforcing bars yielded as they moved from compression to tension, and the covering concrete on the opposite side, where the fiber stress changed from tension to compression, also collapsed simultaneously. Then, during the phase of increasing axial compression, the longitudinal reinforcing bars on the tensile side of the pile yielded for the first time at the cycle with a drift angle of 4/200. At the cycle with a drift angle of 6/200, the hoops started to yield. At the last cycle with a drift angle of 10/200, the longitudinal reinforcing bars in tension failed when the axial force changed from compression to tension.

b) Numerical analysis model

We model the specimen using a cantilever beam as in the analysis of the type-1 pile specimen. The element length is three times larger than the spacing between two adjacent hoops on the basis of the results of a series of the numerical examinations for plastic buckling of the reinforcement as shown in **Fig. 7**. The average stress-strain relation for the swelled reinforcing bars was based on the post-buckling behavior obtained using equivalent linear springs for the hoop resistance in **Fig. 9**. As can been seen in **Fig. 9**, the post-buckling behavior of longitudinal reinforcement in the arrangement in the type-2 pile specimen does not depend on the mechanical properties of the springs representing the hoop resistance.

We set the necessary sectional parameters and material parameters for the constitutive model of longitudinal reinforcement just as in the simulation used for the type-1 pile specimen. The hardening rigidity E_1 is set at one hundredth of the initial rigidity (Young's modulus) E_0 which is compatible with the order

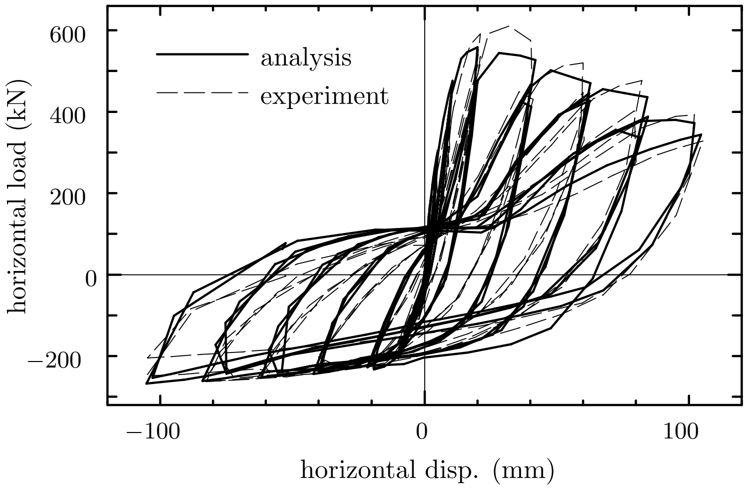

Fig. 17 Horizontal load-horizontal displacement hysteresis at the loading point (type-2 pile specimen)

of the gradient between the yield point and the failure point measured in the material element test. The parameter values for the constitutive model of the covering concrete are the same as those in the numerical simulation for the type-1 specimen.

c) Numerical results and discussion

In the numerical analysis, the horizontal displacement and axial load are input simultaneously. Of course, it is recommended to input the axial load corresponding to the horizontal reaction force just as it was in the experiment explained in **Fig. 16**, but the software used does not provide a subroutine that allows such a scheme. Therefore, we determine the axial load history by trial and error through parametric numerical analysis with respect to several cases of axial load history in order to minimize the discrepancy in hystereses of the horizontal reaction force and axial load at each loading point between the numerical results and the experimental ones. The calculated axial load-horizontal load hysteresis is shown by the solid line in **Fig. 16** together with the original setting in the experiment.

The calculated horizontal load-horizontal displacement hysteresis is shown in **Fig. 17**. Both the envelope and the loop curves fit well with the experimental data. The non-symmetric shapes of the envelope and loops, as caused by the varying axial force, are also well simulated, demonstrating the success of this scheme to take such experimental variations into account in the numerical analysis. However, the load at the final cycle of drift angle is overestimated on the negative side. In the loading state with negative horizontal displacements and axial tension force at this cycle, the longitudinal reinforcement fractured in the experiments. However, since the constitutive model of the reinforcement in the numerical analysis does not include any failure criteria, such a fracture could never be predicted—so the load may be overestimated at that time.

Fig. 18 shows the simulated damage results for the specimen at the cycle with a drift angle of 10/200. This figure is drawn such that the compressive axial force increases as horizontal displacement is applied in the right-hand direction. The predicted pattern of damage distribution is quite similar to the experimental results and is non-symmetric. Although the area of damage in the experiment is slightly broader in the longitudinal direction compared with the numerical results, the patterns of collapse of the covering concrete are identical in the simulation and experiment, with the concrete crushing and falling away. Judging from these results, we can conclude that this numerical model can simulate well the development of progressive damage observed typically in experiments, and that the method of taking into account the effects of variations in axial load is appropriate.

As for damage progress within the cross-section at the bottom of the pile, in the numerical simulation, the covering concrete collapses at the position of an outermost reinforcing bar during the cycle with a drift angle of 6/200, and swelling of an extreme longitudinal reinforcement bar begins in the 8/200 cycle of the

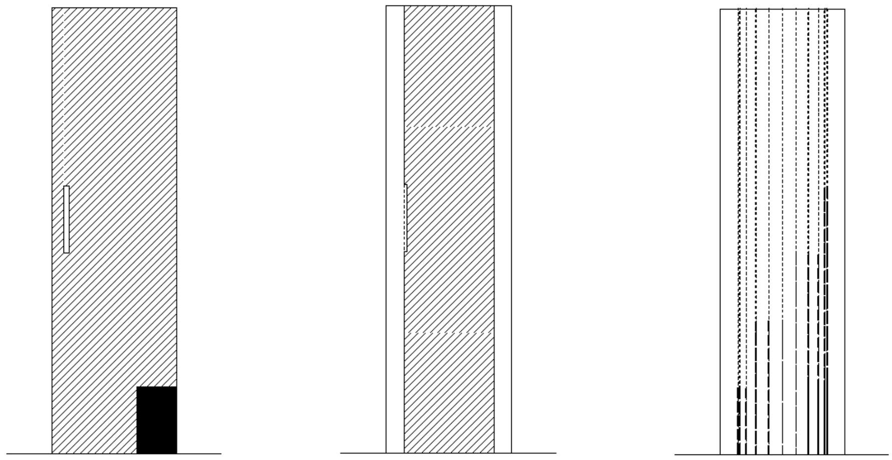

Fig. 18 Estimated damage after final cycle

drift angle. On the other hand, in the experiment, the yielding of a hoop was detected in the cycle with a drift angle of 6/200, and we can assume the occurrence of great damage to the covering concrete at this time. This comparison allows us to conclude that the evolution of damage within the section is also predicted well by the numerical analysis. Namely, accurate simulation of the behavior of this pile from the elastic region to postpeak conditions is possible in our particular analysis, mainly because damage progress in the covering concrete in the longitudinal direction as well as within the section is quite well predicted in accordance with the experimental observations. This indicates again that improvements in the modeling of the covering concrete are one of the most important problems to be solved, as already mentioned in the discussion of numerical analysis results for the type-1 pile specimen in Section **(1)c)**.

Based on the numerical results obtained in these two verification experiments, we can declare that the proposed model is able to estimate the mechanical properties of cast-in-place RC piles to high accuracy no matter what the details of the piles. This makes the proposed method a powerful tool for tracing the behavior of such piles from the elastic to the postpeak states consistently. Of course further studies are necessary to improve the accuracy of the numerical simulations; e.g. it is true and very important that we need to elaborate certain points related to the proper criteria for reinforcing bar swelling. In particular, a more suitable stress-strain relation for the covering concrete must be modeled so that the sustaining branch path of maximum compressive stress and the falling gradients can be appropriately and quantitatively represented.

5. SEISMIC RESPONSE ANALYSIS OF A PILE FOUNDATION

In order to investigate the feasibility of using the proposed model in dynamic analysis, several analyses of a system consisting of a pier, pile foundation, and ground are carried out. In these simulations, several effects are examined including the so-called kinematic interaction between piles and the ground during severe earthquakes. Moreover, special emphasis is placed on the effect that bending damage caused deep in the pile by seismic-motion induced ground displacement has on the response of the superstructure. In carrying out the simulations, the finite element is formulated within the framework of infinitesimal displacement theory.

The object of the examination is a highway bridge pier with a group-pile foundation. **Fig. 19** shows the geometry of the pier and the foundation. This particular foundation was originally introduced in the literature [26] as an example for the ductility design of bridge foundations based on the Specifications for Highway Bridges in Japan [1], [2]. The foundation comprises 4×3 cast-in-place RC piles, the dimension of each of which is 1000 mm in diameter (D) and 23 meters long. The minimum distance between the

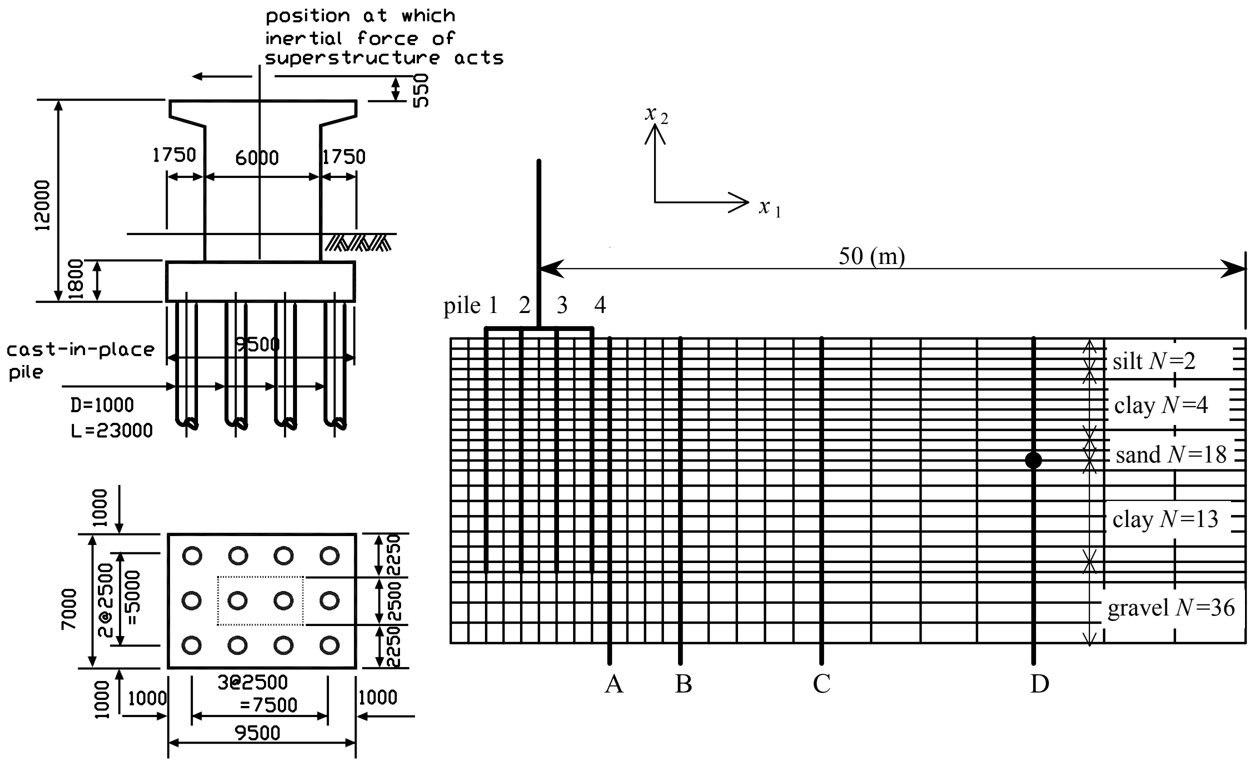

Fig. 19 Simulated pier [26] and finite element mesh

Table 3 Ground profiles

layer	depth (m)	soil	SPT-N	V_{s0} (m/s)	density ρ (t/m^3)
1	4∼7	silt	2	130	1.6
2	7∼14	clay	4	160	1.6
3	14∼16	sand	18	210	1.7
4	16∼26	clay	13	240	1.7
5	26∼34	gravel	36	260	2.0

center of neighboring piles is 2.5D. They are embedded in soft ground classified as Class III as defined in the Specifications. The assumed ground level for seismic design is GL −4 m in compliance with the Specification, this corresponds to the bottom of the footing.

The finite element mesh to be analyzed is also shown in **Fig. 19**. The mesh is actually symmetrical about the center line. The ground conditions used here are simplified for ease of setting the numerical parameters of the ground, as listed in **Table 3**, in comparison with the original settings in the literature [26]. The characteristic period of this simplified ground is evaluated as 0.6 s by the Specifications. Namely, this ground is considered to be relatively hard for Class III ground, because this period classifies it near the boundary between Class II and III. Class II ground has a shorter characteristic period than Class III ground.

The seismic analysis is performed to determine response in the direction perpendicular to the bridge axis. We execute the three types of simulations summarized in **Table 4**. Case 1 models the details of the referenced pier-foundation system as strictly as possible. Case 2 is a modification of Case 1 as follows: the pier material is made elastic; the amount of reinforcement in the piles is much reduced, so the foundation is placed under greater stress than that in Case 1; and the acceleration of the input earthquake wave at the base is 2.2 times larger than that used in Case 1, with this value set by trial and error such that postpeak behavior of bending capacity would be observed deep in the piles. Case 3 is another modification of Case 1, in which further modifications are added to those in Case 2. The differences from Case 2 are as follows:

Table 4 Summary of computational cases

	Case 1	Case 2	Case 3
pier	nonlinear	linear	linear
bearing capacity at tip of pile	nonlinear	linear	linear
arrangement of piles	–	reduced	reduced
amplitude of base input acceleration	×1.0	×2.2	×2.0

the upper limit of bearing capacity at the top of the pile is released to make the compressive axial force on the piles large; and the acceleration of the input earthquake is made twice that used in Case 1 for the same reason as in Case 2. The arrangement of the reinforcement in the piles in the three cases is listed in **Table 5**.

A plane strain element is employed to model the ground for simplicity. This simplification does not result in any problems, because the main purpose of this dynamic analysis is to grasp the characteristics of the relationships between pile damage caused by seismic ground vibration and the behavior of the superstructure-pier-foundation system as a whole. The depth of the element in the out-of-plane direction is twice the depth of the footing in that direction, which is identical to the arrangement employed by Tateishi et al. [9] who reported a seismic dynamic simulation for the same pier. As for the boundary conditions, both edges of the modeled ground are free to move in the horizontal direction but are restrained in the vertical direction, while the motion at the bottom is fixed in both the horizontal and vertical directions.

We employ Hooke's law as the constitutive relation for the soil, and take the nonlinear characteristics of soil into account by changing the instantaneous shear modulus according to the stress history step by step. This instantaneous shear modulus is here given by the Ramberg-Osgood model in terms of the stress history of σ_{12}, where the Cartesian coordinate system x_1-x_2 is set as indicated in **Fig. 19**. However, since this kind of model cannot include strength parameters of soils, the stress level continues increasing in the elements which undergo large strains. Hence the resistance of the ground to the foundation is overestimated when the foundation response becomes relatively large. This situation is one of the problems in our simulation to be solved in the future. Discussions will be necessary as to how the parameters for nonlinear properties in the Ramberg-Osgood model are chosen, and on how to choose a nonlinear constitutive model of the soil.

The initial shear modulus G_0 of the soil in each layer is determined by the phase velocity of shear waves in the corresponding layer, as listed in **Table 3**. Poisson ratios are set at 0.49 independently of the soil properties. Parameters for the nonlinear properties in the Ramberg-Osgood model are estimated by the usual procedure based on the maximum damping constant and the reference strain [27]. We assume that the maximum damping constants of sand and clay are 0.3 and 0.2, respectively. The reference strain ε_r is set to strain ε_{12} when G/G_0 reaches 0.5, where G is the secant shear modulus. The reference strain in each layer is estimated on the basis of existing experimental studies by Iwasaki et al. [28], [29], where the reference strain is determined from the soil profile and the confining pressure. We evaluate the confining pressure at the depth of the gravity center in each element, with the static earth pressure coefficient fixed at 0.5.

The heads of the piles are rigidly connected to the footing. Since plane strain analysis is to be carried out, the three piles in one row are gathered together into one beam.

The same plastic buckling analysis is carried out for the longitudinal reinforcement as in Section **3.**, for each sectioned reinforcement arrangements, and the hoops are modeled by elastic and perfectly-plastic springs. A series of numerical tests determined that the length of the reinforcing bar which shows the most drastic reduction in load after buckling is three times the spacing between two adjacent hoops for all reinforcement arrangements. However, because of the requirement for connecting the fiber elements of piles to the plane strain elements of soils, as will be described later, it becomes much easier to do implement the mesh if the length of a fiber element is equated to the thickness of a plane strain element for the soil.

We therefore carry out the same series of numerical plastic buckling analyses again under the condition

Table 5 Arrangement of reinforcement in pile

GL (m)	Case 1	Case 2, 3
$-4.0 \sim -6.0$	Arrangement 'a'	Arrangement 'c'
$-6.0 \sim -12.0$	Arrangement 'b'	Arrangement 'd'
$-12.0 \sim -18.5$	Arrangement 'c'	Arrangement 'd'
$-18.5 \sim -27.0$	Arrangement 'd'	Arrangement 'd'

Arrangement	longitudinal	hoop
a	SD295 22-D32	SD295 D19 ctc 150
b	SD295 22-D32	SD295 D16 ctc 150
c	SD295 11-D32	SD295 D16 ctc 150
d	SD295 11-D22	SD295 D16 ctc 150

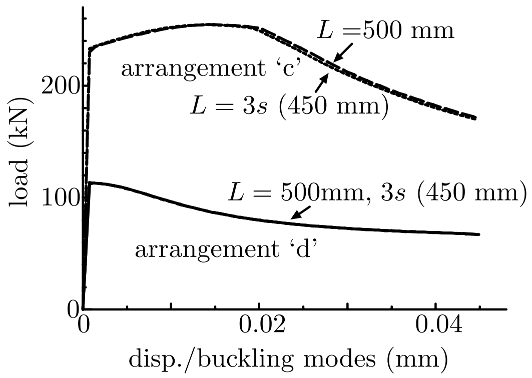

Fig. 20 Numerical analysis of plastic buckling of longitudinal reinforcement bar (arrangements 'c' and 'd')

that the length of the longitudinal reinforcing bars is equal to the depth of the plane strain elements for the ground; i.e. 500 mm. As a typical numerical result, a comparison of the load-displacement relations at the loading point is shown in **Fig. 20** for arrangements 'c' and 'd' in **Table 5** with analyzed lengths $L = 3s = 450$ mm and 500 mm. Discrepancies due to differences in analyzed length are barely discernible in the results for both arrangements. This same tendency is also seen in the numerical results for arrangements 'a' and 'b'. In the case of arrangement 'd', the two curves in **Fig. 20** are too close to be distinguished. We therefore determine that the length of the fiber elements will be 500 mm and that the corresponding post-buckling behavior will be treated as swelling behavior.

Other parameters necessary for the piles are given in the same manner as for the simulations of experiments described in Section **4.**, where the design compressive strength of the concrete is 24 N/mm^2.

We introduced joint spring elements between piles and ground at nodes having identical coordinates. These joint spring elements resist forces in the horizontal and vertical directions. The horizontal joint elements are linear springs with large rigidity so that the relative horizontal displacements and velocities between the piles and the ground are small enough to be ignored.

The vertical joint springs are classified into two types; one type is arranged around the circumference of the pile, while the other is fitted to the pile tip. The former joint springs represent vertical skin friction between pile and soil are a series of discrete elastic-perfect plastic springs. Each is an integrated component of a distributed spring with a constitutive law of elastic and perfectly-rigid-plastic type with strength equal to the maximum skin friction. The subgrade reaction coefficients of the distributed springs are evaluated using an empirical equation from the design code for caisson foundations, while the maximum skin friction is calculated from another empirical equation for cast-in-place RC piles given in the design code. These empirical equations involve SPT-N values.

On the other hand, the vertical joint springs located at the tips of the piles are assumed to be nonlinear elastic. They have a bi-linear response to compression with a maximum strength equivalent to the bearing capacity at the pile tip, but they have no resistance to tension. The compressive spring constant is estimated from the vertical subgrade reaction coefficient, which is considered in the design of caisson foundations, while the maximum strength is derived from an empirical equation for the design of cast-in-place RC piles. Note that, in Case 3, the maximum value of bearing capacity at the tip of pile is ignored. Further, we also combine the three joint elements of three piles in the same row into a single joint element at each depth.

The upper structure system is modeled as a single lumped-mass. The pier is modeled as a single lumped-mass at its middle point and an elastic beam element. The entire section is considered effective, and Young's modulus of concrete is used in calculating the bending rigidities of the beam elements. However a plastic-hinge region based on the Specifications [1] is specified at the bottom of the pier only in Case 1. This plastic-hinge is modeled as a nonlinear rotational spring, the resistance of which is given by a somewhat modified nonlinear relation of the Takeda model [30]. In this modification, the crack point is neglected; the yield bending capacity of the pier is given according to the Specifications [1]; and the tangent bending rigidity after initial yielding is set to 1/10,000 of the initial bending rigidity. The footing is modeled as an elastic beam element with excessive rigidity, and its mass is located as a lumped mass at its gravity center.

As global damping, Rayleigh damping is assumed, and the coefficients corresponding to the 1st and 2nd modes are both set to 3%. An eigenvalue analysis of the whole system gives the first and second eigen periods, where we use the initial rigidity of all the structural members and soils in the calculation. The resulting characteristic periods are 0.52 s for the first mode and 0.38 s for the second. In the first mode, the shear deformation of the ground is greater, and the displacements of ground and structure are in phase. But the second mode is mainly governed by rocking motion of the structure, and the corresponding phases are opposed to each other. We can conclude that the characteristic period of the structure T_s is shorter than that of the ground T_G. This is also supported by the fact that the period of the ground derived according to the design Specifications is 0.6 s. Note that the initial damping matrix at $t = 0$ s is always used in seismic response analyses, because we can expect that most of the damping effect in seismic response analysis arises from hysteresis damping of the foundation materials because of putting the large earthquake motion.

(1) Results of dynamic analyses

The basic input earthquake motion is the NS component of one of the most commonly used earthquakes records, that taken at the Japan Meteorology Agency in Kobe during the Hanshin-Awaji earthquake (the Kobe earthquake) in 1995. In the dynamic analysis, the magnitude of this basic input wave is multiplied by a specific value, and then the adjusted motion is input directly into the nodes of elements at the base. Since the numerical results obtained in Cases 2 and 3 are quite similar to each other, only the results for Cases 1 and 2 are explained in detail below.

a) Dynamic behavior of ground

Fig. 21 shows the distributions of peak displacement of the ground at different positions, where the symbols A through D indicate the observation lines labeled A through D in **Fig. 19**. The same symbols will be used throughout. The peak values in **Fig. 21** are the maximum absolute values. The seismic design code for railway structures [7] introduces empirical equations to estimate distributions of horizontal ground displacement in the depth direction under design seismic motions for bedrock as specified in the code. The corresponding commentary explains that the equations are derived through a statistical compilation of many dynamic analysis results for many ground conditions. Examination of this railway code suggests that the characteristics of L2 motion and Spectral II design seismic motion are very close to our inputs into the numerical simulations. Therefore, in order to evaluate the effect of earthquake motion on the foundation as obtained in our seismic simulations from a practical design point of view, it is very helpful to compare the horizontal displacement of the ground numerically obtained here to that calculated using the empirical equation given in the railway code. This calculation from the code turns out to be approximately 0.2 m, so the ground displacement obtained in Case 1 is of the same order as this value obtained by usual

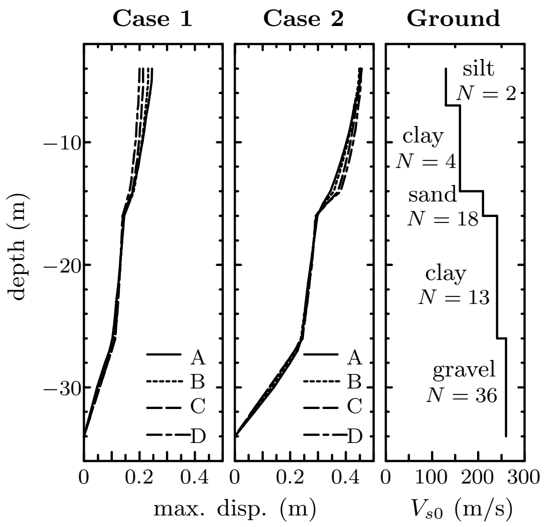

Fig. 21 Distribution of peak ground displacement

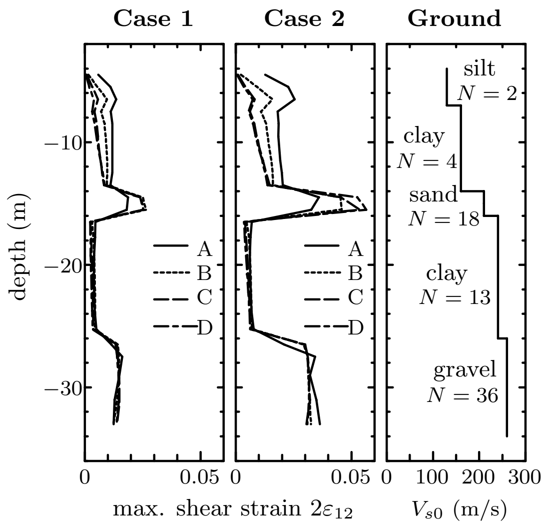

Fig. 22 Distribution of peak shear strain in the ground

design practice for severe earthquakes in Japan. However the displacement obtained in Case 2 is much more severe than that generally assumed in the seismic design of foundations.

Although there is a sudden increase in ground displacement across the boundary from the fourth clay layer to the third sand layer, the increment in displacement is small at the transition from the third sandy layer to the second clay layer. We can also see the same tendency in the distribution of the maximum shear strain, as is shown in **Fig. 22**.

Many attempts have been made to predict the distribution of seismically induced horizontal displacement of the ground, as well as to evaluate the relations between ground profiles and damage locations in piles deep underground. Most treat the ratio of phase velocity V_{s0} in neighboring soil layers as a parameter, because transmission of shear wave causes vibration of the ground. We here follow the same procedure using phase velocities. Ratios of initial shear wave velocities in our settings are calculated to be 0.88 between the fourth and third layers and 0.76 between the third and second ones, where the ratios are obtained by dividing the velocity of the upper layer by that of the lower layer. It is usually considered that the smaller this ratio then the larger the increment in shear strain becomes, because small value indicates low shear rigidity at the upper layer. However, the results for the increment in shear strain obtained by our finite element analyses show the opposite characteristics. We infer that this disagreement with the usual result is caused by differences in the nonlinear characteristics of clay and sand. Consequently, we need to take into account not only the ratio of phase velocities in two adjacent soil strata but also the soil properties when we investigate the distribution of seismic ground displacement under level 2 earthquakes or the relation between soil strata and the distribution of damage to piles deep underground.

We can compare distributions of horizontal displacement and shear strain of the ground at different horizontal positions in the region between the lines A and D in **Figs. 21** and **22**. This shows that the differences in response are big near the ground surface but very small deep underground below GL −15 m. This indicates that the response of the piles near the ground surface is influenced by the inertia of the superstructure as well as the free ground vibration, and this affects the ground motions. Deeper below the surface, on the other hand, the displacement of the piles is mainly caused by seismically induced ground displacement, and does not reflect on the vibration of the ground.

b) Response and damage to foundation in Case 1

Fig. 23 compares a number of time histories: horizontal displacement at the ground surface on line D indicated in **Fig. 19**; horizontal displacement and acceleration of the superstructure at the position where the inertial force acts; the horizontal acceleration of the footing gravity center; the bending moment at

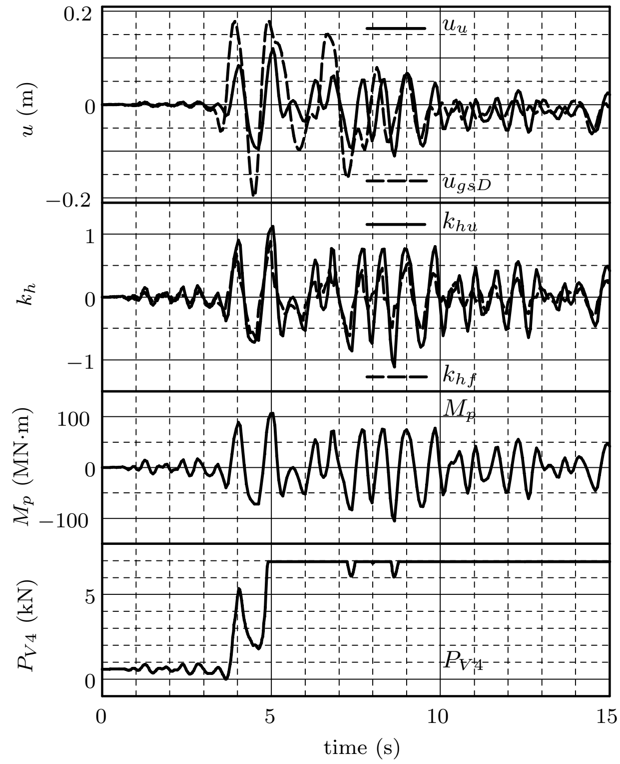

Fig. 23 Time histories of: horizontal displacement at the ground surface on line D u_{gDs}; displacement and lateral force coefficient of the upper structure u_u and k_{hu}; lateral force coefficient of the footing k_{hf}; bending moment of the pier at the bottom M_p; and reaction force at the tip of pile No. 4 P_{V4} (Case 1)

the bottom of the pier; and the reaction force at the tip of pile No. 4. Here the lateral force coefficient is defined by the horizontal acceleration divided by -9.8 m/s^2, and the reaction force at the tip of pile No. 4 is reckoned as positive when it is in compression. Note that the reaction force at the tip of pile No. 4 is chosen as a parameter because it changes accordingly to the tilting moment at the top of the foundation and thus has a strong relationship with the inertial force of the superstructure. From this figure, clearly, the motions of superstructure, ground surface, and footing are in the same phase. The timing of the maximum of each parameter is 4.50 s for ground surface displacement, 5.04 s for lateral force coefficient of the superstructure, 5.04 s for bending moment of the pier at the bottom, and 4.90 s for reaction force acting on the pile tip, respectively. Namely the maxima of superstructure inertial force and displacement of the ground surface are not achieved simultaneously at all, but, when the lateral force coefficient of the superstructure reaches its maximum, the magnitude of ground surface displacement is almost equal to its own maximum value. Consequently, we can in fact regard the maximum inertial force from the superstructure and the maximum ground displacement to occur at the same time and to be in phase.

Next, we discuss the distribution of damage to the pier and foundation during the earthquake in order to understand the general characteristics of damage distribution in the foundation and factors affecting such damage. The bottom of the pier behaves elastically except for short periods when it becomes plastic at maximum bending moment. The response ductility factor of the pier is 1.34, where this is estimated from the horizontal displacement of the center of mass of the superstructure where the inertial force is acting. This indicates that we can assume elastic behavior of the pier on evaluation of the performance of the foundation.

In all piles, tension cracks are observed in the covering concrete over the whole surface. On the other hand, compressive failure never occurs, and hence no swelling of the reinforcements appears.

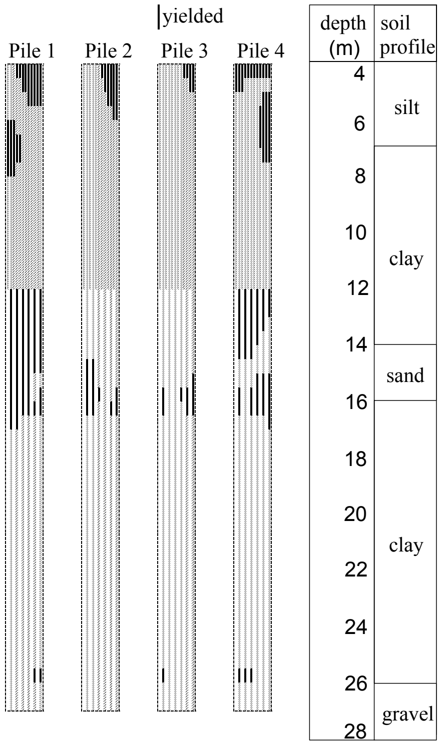

Fig. 24 Yield zone of longitudinal reinforcing bars by tension in piles (Case 1)

As for the longitudinal reinforcement of the piles, **Fig. 24** depicts the distribution of tensile yielding. The gray lines indicate the reinforcement positions, and the black lines represent yielded portions. This tensile yielding occurs not only at the pile tops but also near the boundary of the third sand layer and the fourth clay layer at GL −16 m. The longitudinal range of this yield region is approximately one pile diameter above and below the boundary. Moreover, yielding is observed in a narrow band at a position right above the ground base layer. Namely, deep underground, the reinforcement yields near the boundary between different layers, where the vertical distribution of horizontal displacement and shear strain of the ground abruptly changes.

It can be seen that similar yielding develops near the boundary between the second and third layers of soil strata at GL −14 m. But the distribution of horizontal displacement and shear strain of the ground does not exhibit a sudden change there, as is clear in **Figs. 21** and **22**. We can then conclude that the primary reason of yielding is not only the effect of ground excitation but also abrupt changes in the rigidity and capacity of the piles, since there is a reduction in reinforcement at GL −12 m.

The yield zone at the top of the piles differs depending on the position of the pile. Further, even at the top of the piles, we notice a non-symmetrical distribution of yield zone about the longitudinal centerline of the pile. On the contrary, around GL −16 m, there is almost no difference in yield zone among piles, whether near the center or at the extremity. These results indicate that the dominant factors governing yield are different dependent on depth; yielding at the top of piles is triggered by the inertial force of the superstructure, while that near GL −16 m is affected by the seismic ground displacement.

Furthermore, compressive yielding occurs in Nos. 1 and 4 piles around their circumference at GL −16 m as well as in the central parts at the top. Remember that the bending moment in piles is dependent not only on the bending deformation but also on the axial force, as the experimental results in Section **4.(2)** made clear. Thus, the reason for compressive yielding becoming possible only in the reinforcement of Nos. 1 and 4 piles is thought to be that the axial forces on surrounding piles become larger, and that the bending moment in these piles then exceeds that in the central piles.

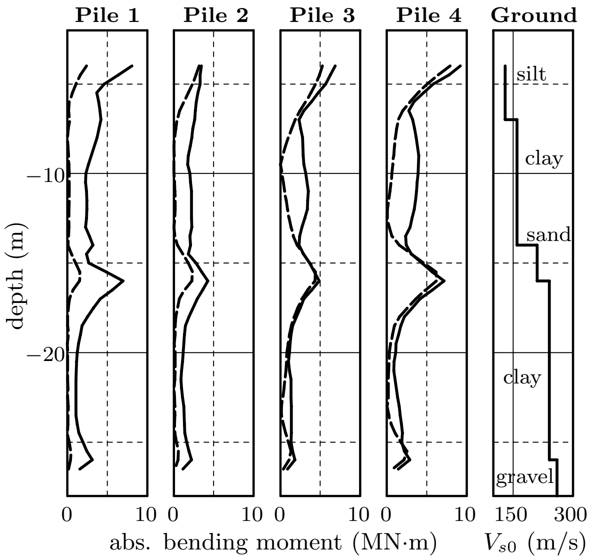

Fig. 25 Distribution of bending moment in each pile (Case 1); solid lines are the absolute maximum values, and dashed lines are the values when the compressive reaction at the tip of No. 4 pile reaches a maximum ($t = 4.9$ s)

Fig. 25 compares the distributions of absolute values of maximum bending moment achieved at each position during the earthquake (solid curves) and of absolute bending moment (dashed curves) when the compressive reaction force at the tip of pile No. 4 reaches a maximum; i.e. at $t = 4.9$ s. The former indicate that all piles experience large bending moments at the top as well as near the boundary between the third sand layer and the fourth clay layer.

The large bending moments deep below the surface are observed at the location where sudden changes in horizontal displacement and ground shear strain appear, as shown in **Figs. 21** and **22**, and these locations are identical to where the pile reinforcement yields. These results imply the possibility of establishing a simple prediction method for pile damage locations without carrying out a sophisticated seismic response analysis of the system consisting of pile foundation and foundation ground as carried out here. That is, by simply referring to a database of dynamic analysis of foundations under several ground conditions when subject to level 2 earthquakes, we may be able to determine the positions of possible damage from the phase velocity profile of the soil strata and the properties of the soil layers; e.g. sandy or clay.

On the other hand, the dashed curves in **Fig. 25**, representing the distribution of pile bending moment when pile No. 4 reacts to the maximum compressive reaction force, clearly indicate that there arises almost no matching bending moment in Nos. 1 and 2 piles. Incidentally, **Fig. 26** shows the distributions of axial force in the piles at that same instant, revealing that almost no axial force appears in these piles, either. The time histories of horizontal ground displacement at GL −16 m on the line D, which corresponds to the solid circle in **Fig. 19**, and the sectional forces and curvature of pile No. 4 at GL −16.25 m are shown in **Fig. 27**. In these time histories, the bending moment has clearly different amplitudes in the positive and negative directions depending on the axial force, while the curvature of the same pile and the horizontal ground displacement oscillate with almost the same magnitude in both directions. This results from the fact that the bending moment of the piles is greatly affected by the axial force. As a result, we can put great emphasis on the advantage of employing a fiber element; i.e. the element can automatically take into account the influence of varying axial force on the mobilized sectional forces of piles.

c) Response and damage to foundation in Cases 2 and 3

Fig. 28 shows the state of damage in the Case 2 simulation. Gray lines indicate the reinforcement again. Here, more reinforcement than in Case 1 yields over the whole pile body, because in Case 2 the amount of reinforcement is reduced. Furthermore, the damage is much more serious lower down than at the top especially near the boundary between the third and fourth soil layers where some damage is also observed

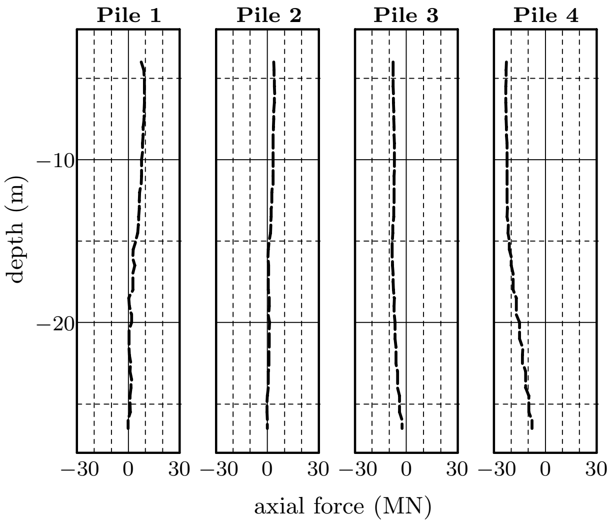

Fig. 26 Distributions of axial force on piles when the reaction force at the tip of pile No. 4 reaches a maximum, $t = 4.9$ s (Case 1), where tension is positive

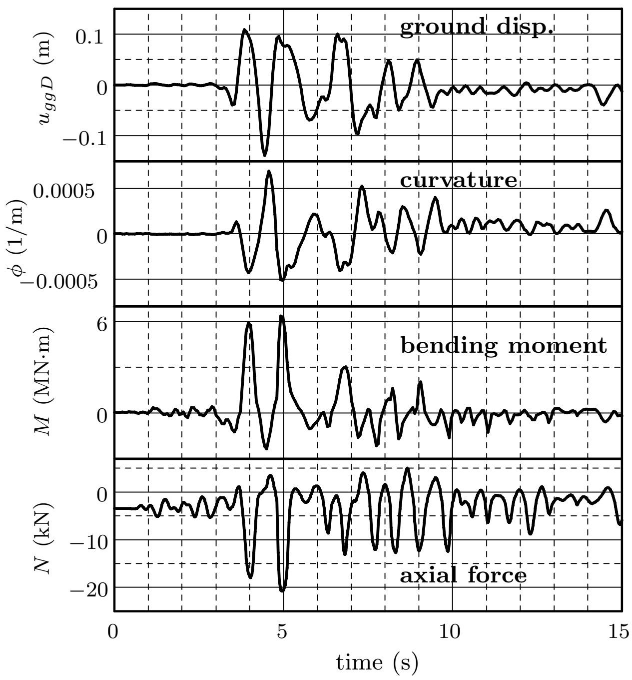

Fig. 27 Time histories of: horizontal displacement of the ground at GL −16 m on line D u_{ggD}; curvature ϕ; bending moment M; and axial force N of pile No. 4 at GL −16.25 m (Case 1)

in Case 1. Near this boundary, it is also apparent that swelling of the reinforcing bars accompanies compressive collapse of the covering concrete. These kinds of damage can also be observed in Case 3.

The stress-strain hysteresis curves in **Fig. 29** are for fibers in the outmost reinforcement bar, which undergoes swelling, as well as for the covering concrete and core concrete surrounding this particular reinforcement bar. The moment-curvature hysteresis of the same element is illustrated in **Fig. 30**. This pile experiences instantaneous swelling of reinforcement several times during the earthquake at this location. Judging from discussion of the results for Case 1, we can conclude that the dominant factor causing this damage is seismic ground displacement. However, it is not very clear from **Fig. 30** that swelling causes tremendous loss of capacity in the pile itself. **Fig. 29** also shows the existence of something like a snap-

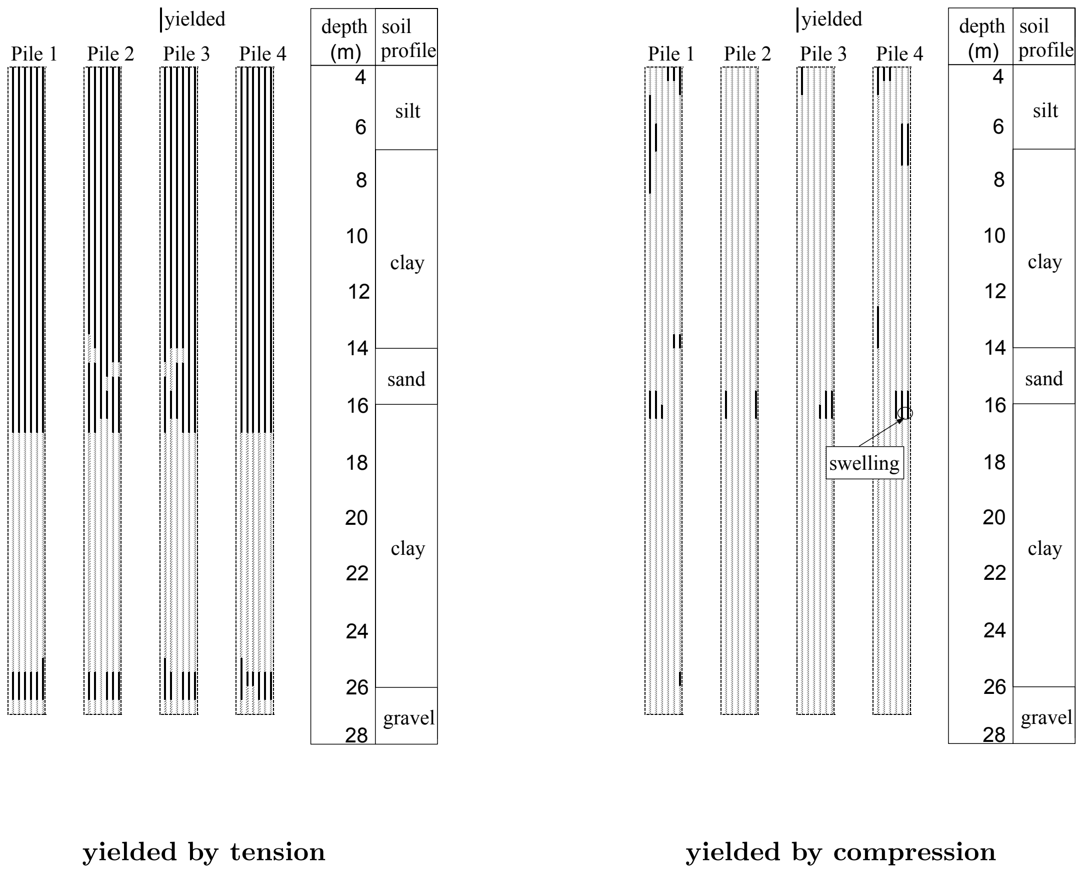

Fig. 28 Yield zone of piles (Case 2)

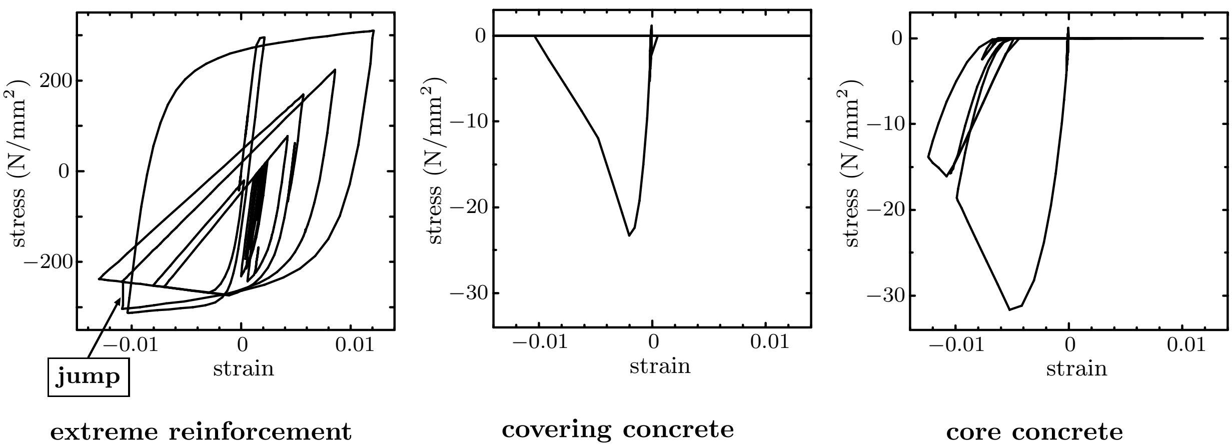

Fig. 29 Stress-strain hysteresis curves of typical fiber element experiencing reinforcing bar swelling

through jump due to swelling along a compressive path in the stress-strain hysteresis of the longitudinal reinforcement. In order to find the cause of this behavior, we examine the time history of strain at that reinforcement. **Fig. 31** shows such a time history from three seconds after the initial state for a period of five seconds. As was assumed in Section **2.(2)**, swelling becomes possible only after a reinforcing bar that has already experienced large strain accompanied with failure of the covering concrete is subjected to compressive re-loading following unloading. In this case, the strain of the longitudinal reinforcement exceeds the compressive collapse strain of the covering concrete $\varepsilon_L = 0.01044$ when the strain suddenly increases at around five seconds. Thereafter tiny oscillations of strain are perceived. We can conclude that

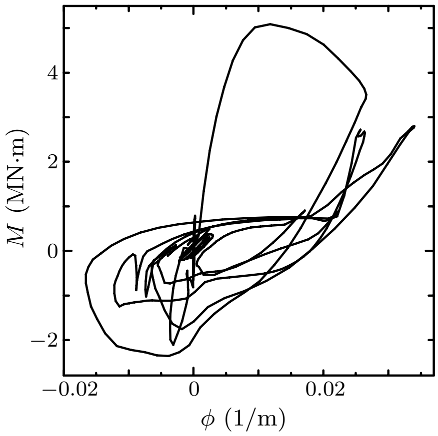

Fig. 30 Bending moment (M-curvature ϕ hysteresis) of an element that contains swelled reinforcement

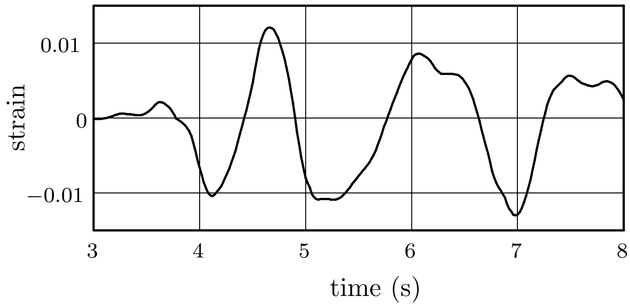

Fig. 31 Time history of axial strain of swelled reinforcement (3 to 8 sec.)

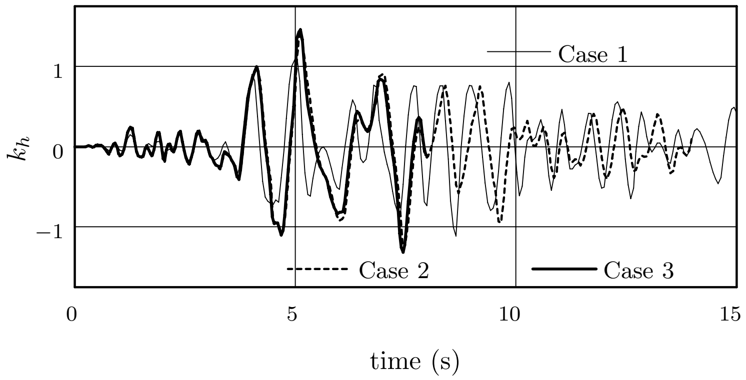

Fig. 32 Comparison of lateral force coefficients obtained in different cases (Cases 1, 2, and 3)

the cause of the jump mentioned above is a short period of consecutive unloading and reloading once the strain of the reinforcement exceeds the failure strain of the covering concrete. Thus the proposed model does not predict a smooth transfer of stress when a pile undergoes such a loading history.

Unfortunately, since experimental data for deformation histories of RC members under the loading paths described above are not available at present, it is not known at all whether such a jump can actually occur in the actual stress-strain hysteresis of reinforcement along such loading paths in RC members or not. Looking at a study by Sakai and Kawashima [31], we may consider that the appearance of minute unloading-loading oscillations in the fibers is one of the general numerical characteristics of dynamic analysis of RC members using fiber elements. However, as will be explained later on, there is no denying the possibility that such a jump in the behavior of reinforcement may lead to difficulty or instability in dynamic analysis. Thus we may still need to improve the hysteresis rule for swelled reinforcement bars further. Moreover, a substantial discussion of the feasibility of fiber elements themselves in the dynamic analysis of RC members may be necessary in the future.

In order to estimate the effect of serious pile damage deep under the surface on the dynamic behavior of the structural system as a whole, we begin by comparing the dynamic response of the superstructure in all numerical cases in **Fig. 32**. In addition, for Case 2, the horizontal response of the superstructure, the ground surface on line D, and the footing are compared in **Fig. 33**.

As **Fig. 32** makes clear, the periods of the Case 2 and 3 responses are longer than that of Case 1 after the maximum response, which occurs at around five seconds. **Fig. 33** shows that the phase difference between superstructure and ground surface in Case 2 is large, especially after $t = 8$ s. These results arise because of plasticization of the piles near the top connection, which is the most critical location as regards supporting

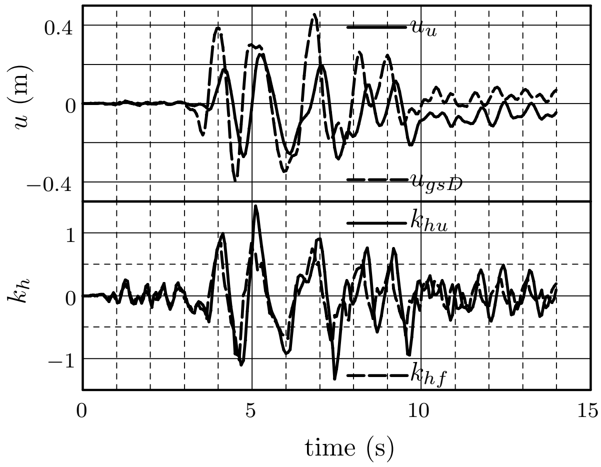

Fig. 33 Time histories of: horizontal displacement of the ground surface on line D, u_{gsD}; horizontal displacement of the superstructure, u_u; lateral force coefficient of the superstructure and footing, k_{hu} and k_{hf} (Case 2)

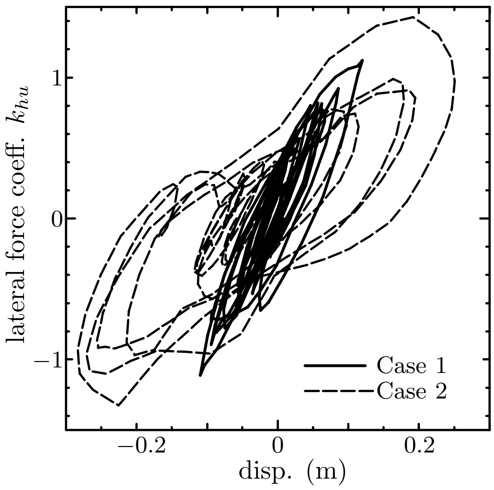

Fig. 34 Hysteresis loops of responding lateral force coefficient versus responding horizontal displacement (Case 1 and 2)

the horizontal forces imposed by the superstructure, as this makes the global period of the entire structure T_s long.

Fig. 34 compares loops of lateral force coefficient versus horizontal displacement of the superstructure between Cases 1 and 2. Regardless of the development of local capacity loss deep under the surface in Case 2, the foundation system retains enough strength for stability. As a result, no phenomenon like progressive tilting in a particular direction is observed. These are thought to be two reasons for this behavior. One is that the surrounding ground can support the horizontal inertial force of the superstructure even after the piles lose capacity. The second is that, since after swelling the damaged portion is forced in the opposite direction by the seismic ground motion, it dose not have a chance to accumulate in only one direction, so the pile maintains an apparent restoring force. Therefore, displacement does not progress in a particular direction.

In **Fig. 32**, the time histories are broken off at 14 s in Case 2 and at 8 s in Case 3, respectively, because the numerical calculations do not converge at these time steps. The magnitudes of both acceleration and displacement are so small here that the numerical problem of convergence error arises as a result of the snap-through jump in the stress-strain hysteresis curve immediately after initiation of swelling, as explained in **Fig. 29**. We also suspect that lack of consideration of the damping effect in the spring at the tip of the pile may be another reason for termination of these calculations, judging from the fact that the response in Case 3 with a linear spring cuts off much earlier than in the Case 2.

(2) Discussion of seismic design of pile foundations including the effect of ground motion

Now, on the basis of the numerical results in Section **(1)**, we discuss a method of seismic design that will prevent damage to piles which may otherwise be induced deep underground by the ground excitation under level 2 earthquake motions.

Our numerical simulations suggest that pile foundations designed according to the current code have adequate resistance to the effect of ground displacement, and that bending damage to piles deep below the surface does not lead to horizontal displacement excessive enough for the girders to fall. Moreover, as far as the authors' knowledge is concerned, past reports of earthquake damage show that, even if liquefaction happens, the collapse or serious displacement of a pile foundation that is property designed to withstand inertial forces is not possible unless the ground experiences a large horizontal residual displacement in one particular direction.

Therefore, we can conclude that the seismic design of foundations of highway bridges requires piles to be primarily designed to resist inertial forces imposed by the superstructures. After that, if we cannot ignore the effect of seismic ground displacement resulting in damage to piles, it is better to carry out the numerical estimate of deformation of the piles subjected to seismic ground vibration, and to give necessary ductility to the piles which may yield. If, in practice, design is to be carried out without any sophisticated numerical analysis which is able to take the effects of seismic excitation of the ground into account, we should specify certain structural details that will improve the toughness of the piles beyond that given by the primary design results.

For example, we recommend that reduction of the section or amount of reinforcement should be avoided for a length equal to twice the pile diameter centering on soil strata boundaries, and that some additional lateral reinforcing must be specified in these regions. These kinds of design modifications can be recommended for the following reason: judging from the seismic response analysis in Section **(1)**, we can predict to some extent the region of damage in advance by standard investigations of the ground; even when reinforcement swelling occurs deep below the surface, the displacement of the pile itself and the pile foundation will not increase abruptly in one particular direction as long as the damaged areas remain able to transfer axial and shear resultant forces. However, further investigation is of course needed in order to specify the possible damage positions and the amount of lateral reinforcement required. We therefore hope that designers and researchers in this field will accumulate such results and combine them with existing knowledge to make an appropriate database available for use when carrying out dynamic finite element analysis.

Since this formulation is within the framework of the infinitesimal displacement theory and material non-linearity of soil is taken into account only by the Ramberg-Osgood model, the effects of large displacements are not included. As a result, the predicted horizontal bearing capacity of the ground may be overestimated. In addition, analysis of plane strain may cause the loss of some three-dimensional effects. Furthermore, we have not discussed what effect the input seismic motion characteristics might have on the numerical results. Hence, further studies of these problems and effects are required in future. In particular, a study of how to set the ultimate state of pile foundations that undergo deep damage as a result of seismic ground excitation needs to be carried out by numerical dynamic examinations of foundation responses when the damage is much greater than obtained in this paper.

6. CONCLUDING REMARKS

With the aim of obtaining consistent simulations of the mechanical behavior of cast-in-place RC piles from the elastic to postpeak states, we have proposed a numerical model based on a fiber elements which takes the effect of reinforcing bar swelling into account. Then we carried out numerical calculations to verify the accuracy of the proposed model, and compared the results with experiments on specimens subjected to cyclic horizontal loading. Next, we conducted a seismic response analysis of a bridge pier with a cast-in-place RC group-pile foundation in order to confirm the feasibility of the proposed model of dynamic analysis. Based on the results of these dynamic numerical simulations, we discussed a seismic design method for pile foundations that can take into account the effects of ground vibration during earthquakes.

The proposed model gives good predictions of the evolution of damage to piles, including the swelling and initiation of rapid bending capacity loss. And the corresponding dynamic analysis also reveals that the proposed method is quite useful for estimating the seismic performance of pile foundations. However, in the present model, there still remain several problems to be solved and improved, especially related to the conditions under which swelling is initiated . For example, we must develop a more suitable stress-strain relation for the covering concrete along the sustaining branch path of the maximum compressive stress, and must establish a modeling method for the degrading gradients of such a constitutive law. In addition, the hysteresis rule for the stress-strain relation of reinforcing bars in the state immediately after swelling may need to be improved further.

The results of dynamic analysis of pile foundations indicate that the effect of bending damage to piles deep below the surface due to seismic ground motion on the restoring force of the whole group-pile foundation is quite small, even when swelling occurs. Therefore, after the usual design procedure for pile foundations to ensure resistance to inertial forces developed by the superstructure, when necessary, the effect of seismic ground displacement should be taken into account by securing enough ductility at predicted yield positions due to ground excitation. Alternatively, a simple design method may in practice be suitable after design for inertial force. For example, this might specify particular structural details that will improve the ductility of piles near the boundaries between soil layers, such as an additional arrangement of lateral confining reinforcement. However, it is still open to further discussions how to set the ultimate limit state accompanying excessive tilting and/or horizontal displacement of foundations.

Eventually, we expect to demonstrate the possibility of establishing a performance-based design method based on ultimate states in which the unstable behavior of pile foundations during earthquakes is examined. As mentioned above, however, we still need to improve the model by resolving the problems revealed above, and to carry out many more numerical analyses to finally clarify the ultimate limit state of bridge foundations.

References

[1] Japan Road Association: Specifications for Highway Bridges V, Seismic Design, 1996.

[2] Japan Road Association: Specifications for Highway Bridges IV, Substructures, 1996.

[3] Fukui, J., Nakano, M., Kimura, Y., Ishida, M., Ookoshi, M., and Banno, A.: Experiments on the ductility of pile foundations subjected to cyclic loading, *Technical Memorandum of PWRI*, No. 3553, Public Works Research Institute, Japan, 1998 (in Japanese).

[4] Kimura, Y., Ookoshi, M., Nakano, M., Fukui, J., and Yokoyama, K.: An experimental study on the ductility of pile foundations, *J. of Struct. Eng.*, JSCE, Vol. 44A, pp. 1597-1606, 1998 (in Japanese).

[5] Public Works Research Institute: Report on the disaster caused by the 1995 Hyogoken Nanbu Earthquake, *J. of Research, PWRI*, Vol. 33, Public Works Research Institute, Japan, 1996.

[6] Research group on seismic design of pile foundations: Report on the effect of ground excitation to pile foundations during severe earthquakes, 2000 (in Japanese).

[7] Railway Technical Research Institute: Seismic design code for railway structures, Maruzen, Tokyo, 1999 (in Japanese).

[8] Murono, Y., and Nishimura, A.: Evaluation of seismic force of pile foundation induced by inertial and kinematic interaction, *12th WCEE*, 2000.

[9] Tateishi, A., and Furuike, A.: A study on seismic performance characteristics of pile foundations estimated by nonlinear dynamic analysis with the effect of the varying axial force, *Proc. of the 25th JSCE Earthquake Eng. Symp.*, pp. 585-588, JSCE, 1999 (in Japanese).

[10] Maekawa, K., Tsuchiya, S., and Fukuura, N.: Nonlinear analysis of reinforced concrete and seismic performance evaluation, *Proc. of the Second Symposium on Nonlinear Numerical Analysis and its Application to Seismic Design of Steel Structures*, JSCE, pp. 1-16, 1998 (in Japanese).

[11] Suda, K., and Masukawa, J.: Models for concrete cover spalling and reinforcement buckling of reinforced concrete, *12th WCEE*, No. 1437, 2000.
[12] Suda, K., Murayama, Y., Ichinomiya, T., and Shimbo, H.: Buckling behavior of longitudinal reinforcing bars in concrete columns subjected to reversed lateral loading, *11th WCEE*, No. 1753, 1996.
[13] Nakamura, H.: An effect of the buckling of reinforcement bar on the postpeak behavior of RC structures, Concrete Engineering Series 20, JSCE, pp. 98-100, 1997 (in Japanese).
[14] Nakamura, H., Niwa, J., and Tanabe, T.: An effect of the buckling of reinforcement bar on the postpeak behavior of RC structures, *Proc. of the JCI*, Vol. 14, No. 2, 1992 (in Japanese).
[15] Gomes, A., and Appleton, J.: Nonlinear cyclic stress-strain relationship of reinforcement bars including buckling, *Engineering Structures*, Vol. 19, No. 10, pp. 822-826, 1997.
[16] Nakamura, H.: Stress-strain relation of concrete as a characteristic of material, Concrete Engineering Series 20, JSCE, pp. 92-95, 1997 (in Japanese).
[17] Tomita, Y.: Overview of elasto-plastic finite deformation analyses by finite element method (localized deformation and numerical simulation), *J. of the Japan Soc. for Tech. of Plasticity*, Vol. 36, No. 408, pp. 2-9, 1995 (in Japanese).
[18] Shirato, M., Kimura, Y., Fukui, J., and Takahashi, M.: A numerical analysis for postpeak behavior of pile foundation, *J. of Struct. Eng.*, JSCE, Vol. 45A, pp. 1387-1398, 1999 (in Japanese).
[19] Menegotto, M., and Pinto, P. E.: Method of analysis for cyclically loaded R.C. plane frames including change in geometry and non-elastic behavior of elements under combined normal force and bending, *IABSE symposium on resistance and ultimate deformability of structures acted on by well-defined repeated Loads, Final Reports*, Vol. 13, pp. 15-22, Lisbon, 1973.
[20] Ristic, D., Yamada, Y., Iemura, H., and Petrovski, J.: Nonlinear behavior and stress-strain based modeling of reinforced concrete structures under earthquake-induced bending and varying axial loads, Research Report, No. 88-ST01, School of Civil Engineering, Kyoto University, 1988.
[21] Ohtsuka, H., Hoshikuma, J., Nagaya, K., and Murai, K.: Experiments of cast-in-place RC piles subjected to cyclic load, *Technical Memorandum of PWRI*, No. 3462, Public Works Research Institute, Japan, 1996 (in Japanese).
[22] Hoshikuma, J., Kawashima, K., Nagaya, K., and Taylor, A. W.: Stress-strain model for confined reinforced concrete in bridge piers, *J. of Struct. Eng.*, ASCE, Vol. 123, No. 5, 1997.
[23] Shirato, M., Fukui, J., and Kimura, Y.: Characteristics of the swelling of longitudinal reinforcements in cast-in-place RC piles, *Proc. of the 25th JSCE Earthquake Eng. Symp.*, JSCE, pp. 569-572, 1999 (in Japanese).
[24] Tanamura, S., Kondoh, M., Kanamori, M., and Sugawara, A.: Cyclic loading tests of model piles with high-strength shear reinforcements, *RTRI Report*, Vol. 12, No. 12, pp. 47-52, Railway Technical Research Institute, Japan, 1998 (in Japanese).
[25] Fukui, J., Nakano, M., Ishida, M., Nanazawa, T., Adachi, T., and Taguchi, H.: An investigation of actual conditions on adoption of types of foundations, *Technical Memorandum of PWRI*, No. 3500, Public Works Research Institute, Japan, 1996 (in Japanese).
[26] Committee on publishing design examples of highway bridges: Useful design example of highway bridges, Civil Engineering Journal, Supplement, April-1998, pp. 121-141, Sankaido, Tokyo, 1998 (in Japanese).
[27] Architectural Institute of Japan: An introduction to dynamic soil-structure interaction, Maruzen, Tokyo, 1996 (in Japanese).
[28] Iwasaki, T., Tatsuoka, F., and Takagi, Y.: An experimental study on dynamic deformation characteristics of soils, Part II – dynamic deformation characteristics of sand in wide range of strain level –, *J. of Research, PWRI*, No. 153, Public Works Research Institute, Japan, 1980 (in Japanese).
[29] Iwasaki, Y., Tokita, K., and Yoshida, S.: Dynamic deformation characteristics of alluvial clays – Strain-dependency of shear rigidity –, *Technical memorandum of PWRI*, No. 1504, Public Works Research Institute, Japan, 1979 (in Japanese).
[30] Takeda, T., Sozen, M. A., and Nielsen, N. M.: Reinforced concrete response to simulated earthquakes, *J. of the Struct. Div.*, ASCE, Vol. 96, No. ST12, pp. 2557-2573, 1970.
[31] Sakai, J., and Kawashima, K.: Nonlinear seismic response analysis of a reinforced concrete bridge column by the fiber element, *J. of Struct. Eng.*, JSCE, Vol. 45A, pp. 935-946, 1999 (in Japanese).